8
Hyperspectral Remote Sensing

Eyal Ben-Dor, Daniel Schläpfer, Antonio J. Plaza, and Tim Malthus

8.1
Introduction

Hyperspectral remote sensing (HRS) and imaging spectroscopy (IS) are the same technologies that provide detailed spectral information for individual pixels of an image. While HRS refers mostly to remote sensing (from a distance), the emerging IS technology covers wide spatial–spectral domains, from microscopic to macroscopic HRS/IS. IS is an innovative development of the charge-coupled device (CCD), which was invented in 1969 by the two 2009 Nobel prize in Physics winners Willard Boyle and George Smith. In 1972, Goetz applied the CCD technology for spectral applications, and after developing the first field portable spectrometer, a combined spatial and spectral capability was designed and successfully operated from orbit (LANDSAT program).

HRS/IS is a technology that provides spatial and spectral information simultaneously. It enables the identification of targets and other phenomena as the spectral information is presented on a spatial rather than point (pixel) basis. HRS/IS are tools with many applications, such as geology, ecology, geomorphology, limnology, pedology, atmospheric science, and forensic science. As such HRS/IS technology is applied by decision makers, farmers, environmental watchers in both the private and government sectors, city planners, stock holders, and others. The use of HRS/IS sensors is still relatively costly and requires professional manpower to operate the instrument and process the data.

Today, in addition to the growing number of scientific papers and conferences focusing on this technology, the HRS/IS discipline is very active: commercial sensors are being built, orbital sensors are in advanced planning stages, national and international funds are being directed toward using this technology, and interest from the private sector increases. The aim of this chapter is to provide the reader with a comprehensive overview of this promising technology from historical to operational perspectives.

Airborne Measurements for Environmental Research: Methods and Instruments, First Edition.
Edited by Manfred Wendisch and Jean-Louis Brenguier.

8.2 Definition

HRS/IS (HRS from now on) provides high spatial/spectral resolution radiance data from a distance. This information enables the identification of targets based on their spectral properties (mainly absorption features of chromophores). This approach has been found to be very useful in many terrestrial, atmospheric, and marine applications (Clark and Roush, 1984; Goetz and Wellman, 1984; Gao and Goetz, 1990; Dekker *et al*. 2001; Asner and Vitousek, 2005). The classical definition for HRS is given by Goetz *et al*. (1985): ''The acquisition of images in hundreds of contiguous registered spectral bands such that for each pixel a radiant spectrum can be derived.'' This definition covers the spectral regions of VIS (visible), NIR (near infrared), SWIR (shortwave infrared), MWIR (midwave infrared), LWIR (longwave infrared), and recently also the UV (ultraviolet). For the specific wavelengths, refer to Table 7.1 in Chapter 7 and Table 8.1. It includes all spatial domains and platforms (microscopic to macroscopic; ground, air, and space platforms) and all targets (solid, liquid, and gas). For this technology, Not only ''high number of bands'' but also high spectral resolution, that is, a narrow bandwidth (FWHM, full width at half maximum), and a large sampling interval across the spectrum are needed. The accepted FWHM for HRS technology is 10 nm (Goetz, 1987). New applications, such as assessing vegetation fluorescence, require bandwidths of less than 1 nm (Guanter, Estellés, and Moreno, 2006; Grace *et al*. 2007).

HRS can also be defined as ''spatial spectrometry from afar'' that adopts spectral routines, models, and methodology and merges them with spatial information. While conditions are constant and well controlled in the laboratory, in the acquisition of high-quality spectral data in airborne/spaceborne cases, significant interference is encountered, such a lower signal-to-noise ratio (SNR) induced by the short dwell time of data acquisition over a given pixel, atmospheric attenuation of gases and aerosol particles and the uncontrolled illumination conditions of the source and objects. This makes HRS a challenging technology that involves many disciplines, including atmospheric science, electro-optical engineering, aviation, computer science, statistics and applied mathematics, and more. The major aim of

Table 8.1 Wavelength ranges applied in HRS.

Name of Range	Abbreviation	Wavelength, λ (μm)
Ultraviolet	UV	0.28–0.35
Visible	VIS	0.35–0.7
Near infrared	NIR	0.7–1
Shortwave infrared	SWIR	1–2.5
Midwave infrared	MWIR	3–5
Longwave infrared	LWIR	8–12
Thermal infrared	TIR	3–50
Infrared	IR	1–1000

HRS is to extract physical information across the spectrum (radiance) to describe inherent properties of the targets, such as reflectance and emissivity. Under laboratory conditions, the spectral information across the UV-VIS-NIR-SWIR-MWIR-LWIR spectral regions can be quantitatively analyzed for a wealth of materials, natural and artificial, such as vegetation, water, gases, artificial material, soils, and rocks, with many already available in spectral libraries. If a HRS sensor with high SNR is used, an analytical spectral approach yields new products (Clark, Gallagher, and Swayze, 1990; Krüger, Erzinger, and Kaufmann, 1998). The high spectral resolution of HRS technology combined with temporal coverage enables better recognition of targets and an improved quantitative analysis of phenomena, especially for land use cover application.

Allocating spectral information temporally in a spatial domain provides a new dimension that neither the traditional point spectroscopy nor air photography can provide separately. HRS can thus be described as an ''expert'' geographic information system (GIS) in which surface layers are built on a pixel-by-pixel basis rather than a selected group of points with direct and indirect chemical and physical information. Spatial recognition of the phenomenon in question is better performed in the HRS domain than by traditional GIS techniques. HRS consists of many points (actually the number of pixels in the image) that are used to generate thematic layers, whereas in GIS, only a few points are used to describe an area of interest (raster vs vector).

Figure 8.1 shows the concept of the HRS technology. Each individual pixel is characterized by a complete spectrum of ground targets (and their mixtures) that can be quantitatively analyzed within the spatial view. The capability of acquiring quantitative information from many points on the ground at almost the same time provides another innovative aspect of HRS technology. It freezes time for all spatial pixels at almost the same point, subsequently permitting adequate temporal

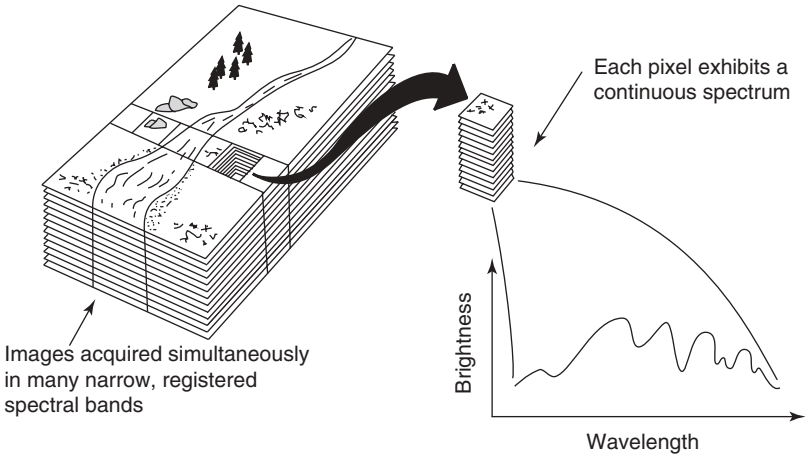

Figure 8.1 The concept of HRS/IS: each pixel element has a continuous spectrum that is used to analyze the surface and atmosphere, after Goetz (1987).

analysis. HRS technology is thus a promising tool that adds many new aspects to the existing mapping technology and improves our capability to remote-sense materials from far distances.

8.3 History

Alex Goetz is considered a mentor and pioneer scientist in HRS technology together with his colleague Gregg Vane. Goetz (2009) and MacDonald, Ustin, and Schaepman (2009) reviewed the history of HRS development since 1970. HRS technology was driven by geologists and geophysicists who realized that the Earth's surface mineralogy consists of significant and unique spectral fingerprints across the SWIR, MWR, and LWIR spectral regions (later the VIS–NIR spectral region was also explored). This knowledge was gained from comprehensive work with laboratory spectrometers and was followed by a physical explanation of the reflectance spectral response of minerals in rocks and soil. Hunt and Salisbury (1970, 1971); Hunt, Salisbury, and Lenhoff (1971a,b); Stoner and Baumgardner (1981); Clark (1999) created the first collection of available soil and rock spectral libraries.

HRS capability leans heavily on the invention of the CCD assembly in 1969 (Smith, 2001), which provided the first step toward digital imaging. These achievements acted as a precursor to establishing a real image spectrometer that would rely on the commercial hybrid focal plane array that was available at that time (in 1979). The first sensor of this kind was used in the shuttle mission SMIRR (shuttle multispectral infrared radiometer) in 1981. In 1983, Goetz and Vane started to build an airborne HRS sensor (airborne imaging spectrometer, AIS), which was sensitive in the SWIR region (Goetz, 2009).

The 2D detector arrays (32×32 elements) consisted of HgCdTe detectors generated images at wavelength greater than 1.1 μm. The array detector did not need a scan and provided sufficient improvement in the SNR to suit airborne applications. The AIS was a rather large instrument and was flown onboard a C-130 aircraft. It had two versions, with two modes being used in each: the "tree mode" from 0.9 to 2.1 μm and the "rock mode" from 1.2 to 2.4 μm.

The instantaneous field of view (IFOV) of the AIS-1 was 1.91 mrad and of the AIS-2 2.05 mrad; the ground instantaneous field of view (GIFOV) (from 6 km) was 11.4 and 12.3 m, and the FOV was 3.7° and 7.3°, respectively. The image swath was 365 m for AIS-1 and 787 m for AIS-2, with a spectral sampling interval of 9.3 and 10.6 nm, respectively. The AIS-1 was flown from 1982 to 1985 and the AIS-2, a later version with spectral coverage of 0.8–2.4 μm and 64-pixel width (Vane and Goetz, 1988), was operated in 1986. In those days, methods to account for atmospheric attenuation were not available; nonetheless, by simple approximation, the sensor and the HRS concept were able to show that minerals can be identified and spatially mapped over an arid-environment terrain. The proceedings of a conference that summarized the activity and first results of the AIS missions were published by

the National Aeronautics and Space Administration (NASA) in 1985 and 1986. At that time, spectral libraries of mineral and rock material had not yet been developed. Rowan proved that the HRS technology was able to detect the mineral buddingtonite from afar and solved the mystery of unrecognized spectral feature at that time.

In 1984, Vane started to build AVIRIS (Airborne Visible and Infrared Imaging Spectrometer). The first developed AVIRIS lasted three years (1984–1987), with its first flight taking place in 1987. Although being a relatively low-quality SNR instrument, the first AVIRIS demonstrated excellent performance relative to the AIS. The sensor covered the entire VIS-NIR-SWIR region with 224 bands (around 10 nm FWHM), with 20 m GIFOV and around 10 × 10 km swath. It was a whiskbroom sensor with a SNR of around 100 carried onboard an ER-2 aircraft from 20 km altitude. Since then, the AVIRIS sensor has undergone upgrades. The major differences are its SNR (100 in 1987 relative to >1000 today), spectral coverage (400–2500 nm vs 350–2500 nm today) and spatial resolution (20 m vs 2 m today).

The instrument can fly on different platforms at lower altitudes and has opened up new capabilities for potential users in many applications. Even today, with many new HRS sensors having become available worldwide, the AVIRIS sensor is still considered the best HSR sensor (Goetz, 2009). This is due in large part to careful maintenance and upgrade of the sensor over the years and to the growing interest of the HRS community in using the data. The AVIRIS program has established an active HRS community in the United States and then in Europe that has rapidly matured. On the basis of this capability and success, other sensors have been developed and built over the past two decades worldwide.

8.4 Sensor Principles

Imaging spectrometers typically use a two-dimensional (2D) matrix array (e.g., a CCD or focal plane array (FPA) that produces a 3D data cube (spatial dimensions and a third spectral axis). These data cubes are built in a progressive manner by (i) sequentially recording one full spatial image after another, each at a different wavelength, or (ii) sequentially recording one narrow image (1 pixel wide, multiple pixels long) swath after another with the corresponding spectral signature for each pixel in the swath. Some common techniques used in airborne or spaceborne applications are depicted in Figure 8.2. The first two approaches shown are basic ones, used to generate images such as those used in LANDSAT (Figure 8.2a) and SPOT (Figure 8.2b). They show the concept of measuring reflected radiation in a discrete detector or in a line array.

Multichannel sensors such as LANDSAT TM are optical mechanical system in which discrete, fixed detector elements are scanned across the target perpendicular to the flight path by a mirror and these detectors convert the reflected solar photons from each pixel in the scene into an electronic signal. The detector elements are placed behind filters that pass broad portions of the spectrum. One approach to

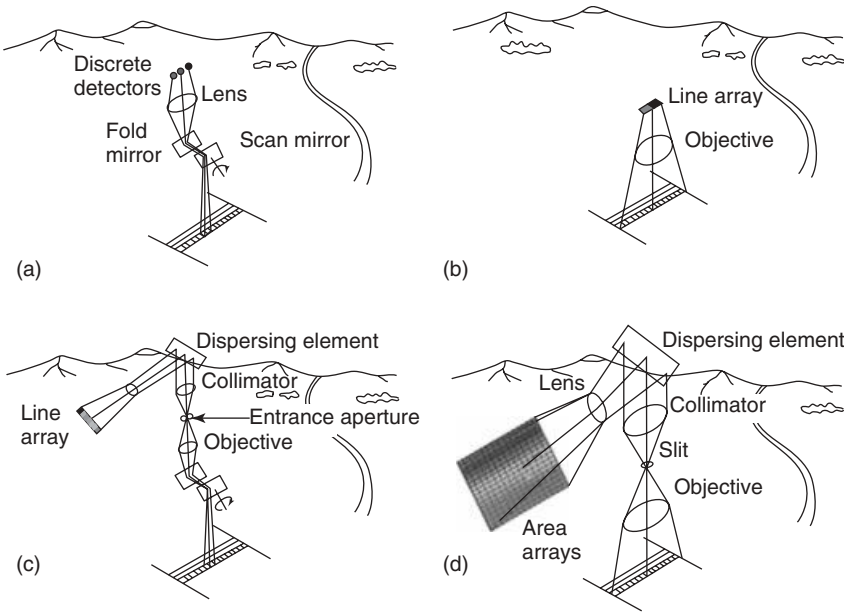

Figure 8.2 Four approaches to sensors for multispectral imaging. (a) multispectral imaging with discrete detectors (LANDSAT type); (b) multispectral imaging with line arrays (SPOT type); (c) imaging spectroscopy with line arrays (AVIRIS type, whiskbroom); and (d) imaging spectroscopy with area array (AISA type, pushbroom). (Source: Taken from Goetz (1987).)

increase the residence time of a detector in the IFOV is to use line arrays of detector elements (Figure 8.2b). This type of sensor is presented by the French satellite sensor SPOT.

There are limitations and trade-offs associated with the use of multiple line arrays, each with its own spectral band-pass filter. If all the arrays are placed in the focal plane of the telescope then the same ground locations are not imaged simultaneously in each spectral band. If a beam splitter is used to facilitate simultaneous data acquisition, the signal is reduced by 50% or more for each additional spectral band acquired in a given spectral region. Furthermore, instrument complexity increases substantially if more than 6–10 spectral bands are desired. Two other approaches to HRS are shown in Figure 8.2c,d. The line array approach is also known as *whiskbroom configuration* and the area array approach as *pushbroom configuration*. The line array approach is analogous to the scanner approach (Figure 8.2b), except that the light from a pixel is passed into a spectrometer where it is dispersed and focused onto a line array. Thus, each pixel is simultaneously sensed in as many spectral bands as there are detector elements in the line array. For high spatial resolution imaging of ground IFOVs of 10to 30 m, this concept is suitable only for an airborne sensor that flies slowly enough so that the integration time of the detector array is a small fraction of the integration time. Because of the high velocities of spacecraft, an imaging spectrometer designed for

the Earth's orbit requires the use of two distinguished area arrays of the detector in the focal plane of the spectrometer (Figure 8.2d), thereby obviating the need for an optical scanning mechanism (pushbroom configuration).

The key to HRS is the detector array. Line arrays of silicon, sensitive to radiation at wavelengths of up to 1.1 μm, are available commercially in dimensions of up to 5000 elements in length. Area arrays of up to 800 × 800 elements of silicon were developed for wide-field and planetary camera. However, the state of infrared array development for wavelength beyond 1.1 μm is not so advanced. Line arrays are available in several materials up to few hindered detector elements in length. Two of the most attractive materials are mercury-cadmium-telluride (HgCdTe) and indium antimonite (InSb). InSb arrays of 512 elements with very high quantum efficiency and detectors with similar element-to-element responsivities have developed. The InSb arrays respond to wavelengths from 0.7 to 5.2 μm. A comprehensive description of both pushbroom and whiskbroom technologies with advantages and disadvantages can be found in Sellar and Boreman (2005).

8.5 HRS Sensors

8.5.1 General

The growing number of researchers in the HRS community can be seen by their attendance at the yearly proceedings of the AVIRIS Workshop Series, organized by JPL since 1985 (starting with AIS, and today with HyspIRI) and other workshops organized by international groups such as WHISPERS (Work group on Hyperspectral Image and Signal Processing: Evaluation in Remote Sensing) and EARSEL SIG IS (European Remote Sensing Laboratory Special Interest Group on Imaging Spectroscopy). In 1993, a special issue of *Remote Sensing of Environment* was published, dedicated to HRS technology in general and to AVIRIS in particular (Vane, 1993). This broadened the horizon for many potential users who still had not heard about HRS technology, ensuring that the activity would continue. Today, new HRS programs are up and running at NASA, such as the M^3 (Moon Mineralogy Mapper) project in collaboration with the Indian Space Agency to study the moon's surface (Pieters *et al*. 2009b), along with preparations to place a combined optical and thermal hyperspectral sensor in orbit, the HyspIRI (Hyperspectral Infrared Imager) project (Knox *et al*. 2010). In addition to the AIS and AVIRIS missions, NASA also successfully operated a thermal hyperspectral mission known as TIMS (thermal infrared multispectral scanner) in circa 1980–1983 (Kahle and Goetz, 1983) and also collaborated on other HRS initiatives in North America. The TIMS and, then later, the ASTER spacecraft sensors showed the thermal region's promising capability for obtaining mineral-based information. Apparently, the thermal infrared (TIR) HRS capability because of its costs and performance was set aside, and it has only recently begun to garner new attention, in new space initiatives (HyspIRI)

and in new airborne sensors (e.g., TASI-600 (Thermal Airborne Spectrography Imager) and MASI-600 (Midwave Infrared Airborne Spectrographic Imager) from ITRES (Innovation Technology Research Excellence and Science), HyperCam from TELOPS, SEBASS (Spatially Enhanced Broadband Array Spectrograph System) from Aerospace Corporation, and Owl from SpecIm). In parallel to the US national HRS activity, a commercial HRS sensor was developed in circa 1980. The Geophysical & Environmental Research Corporation (GER) of Millbrook, New York, developed the first commercial HRS system which acquired 576 channels across 0.4–2.5 μm in 1981, first described by Chiu and Collins (1978). After the GER HRS, came a 63–channel sensor (GERIS-63) that was operated from around 1986 to 1990: this was a whiskbroom sensor that consisted of 63 bands (15–45 nm bandwidth) across the VIS-NIR-SWIR region with a 90° FOV (Ben-Dor, Goetz, and Shapiro, 1994). The sensor was flown over several areas worldwide and demonstrated the significant potential of the HRS concept. Although premature at that time, GER then began to offer commercial HRS services. However, it appears that the market was not yet educated enough and the very few scientists who were exposed to this technology at that time could not support the GER activity. Thus, the GER initiative was ahead of its time by about two decades, and it reestablished its commercial activity in 2000. The GER sensor was brought to Europe in May and June 1989 for demonstration purposes, and a campaign organized by several European users (known as EISAC-89, European Imaging Spectroscopy Airborne Campaign) was conducted. The results of this mission were impressive and pushed the European community to learn more about this technology (Itten, 2007). At around the time of the first AIS mission (1981), the Canadians had also developed an imaging device known as FLI (fluorescence line imager).

In the mid-1980s, Canada Moniteq Ltd. developed and used a limited pushbroom scanner, the FLI/PMI, with 228 channels across 430–805 nm (Borstad *et al*. 1985; Gower and Borstad, 1989). This sensor was also brought to the EISAC-89, and in 1991, the first *EARSeL Advances in Remote Sensing* issue (Volume 1, Number 1, February 1991), which was dedicated to HRS, provided the outcomes of this campaign, demonstrating that atmospheric attenuation, calibration, and validation were the major issues that needed to be tackled. It is interesting to note that most of the authors were satisfied with the results but their demand for more data was blocked by an inability to access data and sensors until DLR (Deutsches Zentrum für Luft- und Raumfahrt, German Aerospace Center) entered the scene. The interest of DLR in HRS began in around 1986 when they announced plans for ROSIS, Reflective Optics System Imaging Spectrometer (a pushbroom instrument offering 115 bands between 430 and 850 nm), which only became operational in 1992 and was continuously upgraded until 2003 (Holzwarth *et al*. 2003; Doerffer *et al*. 1989; Kunkel *et al*. 1991). In 1996, DLR owned and operated the DAIS 7915 (Digital Airborne Imaging Spectrometer) sensor (see further on) and then operated the HyMAP (Hyperspectral MAPping) in several campaigns in Europe and Africa. They recently own the HySpeX sensor, together with GFZ in Germany (2012) that will enable freedom and comfort to operate HSR sensor without leaning on a third party. Both bodies (DLR and GFZ) together with other German groups initiated,

in 2007, a new and ambiguous initiative to place high-quality HRS sensor in orbit, termed Environmental Mapping and Analysis Program (EnMAP; see further on).

On the basis of the growing interest of the European Union (EU) scientific community in HRS technology, especially after the successful EISAC-89 campaign, it was obvious that AVIRIS, the most advanced sensor at that time, would be brought to Europe for a large campaign. AVIRIS was deployed in the Mac-Europe campaign in 1991 (Clevers, 1999) on-board the NASA ER-2 aircraft, and covered test sites in Germany, The Netherlands, France, Iceland, Italy, England, Spain, and Austria (Itten *et al.* 1992). The success of the campaigns on the one hand and the complexity and cost involved in bringing AVIRIS (or any other HRS sensor) on the other were the driving forces for a new initiative in Europe to be independent in term of sensors, data availability, research capacity, and experience. This led to the purchase of HRS sensors by several bodies in Europe: in Germany (Compact Airborne Spectrographic Imager (CASI), by the Free University of Berlin and DAIS 7915 by DLR) and Italy (multispectral infrared and visible imaging spectrometer (MIVIS), by the Italian National Research Council, CNR). In addition, plans were made for the development of more general sensors for the benefit of all European Community (EC) members and were established via the European Space Agency (ESA) Program for the Development of Scientific Experiments (PRODEX) project APEX, Airborne Prism Experiment (Itten *et al.* 2008), and by some limited commercial activities.

The DAIS 7915 was a GER whiskbroom instrument characterized by 72 channels across the VIS-NIR-SWIR region and 7 bands in the TIR region (3.0–12.6 μm). It had a 26° FOV and GIFOV between 5 and 20 m. This instrument was offered in 1996 as a large-scale facility instrument to European researchers and served as a test bed in a large number of international flight campaigns. Although it was not the ideal sensor in terms of SNR and operational capabilities, the DAIS 7915 was operated by DLR until 2002 when it could no longer satisfy the higher SNRs being requested by the community. The experience gained from the DAIS 7915 campaigns was very valuable in terms of opening up the HRS field to more users, developing independent operational and maintenance capabilities, educating the younger generation and opening fruitful discussions among emerging HRS community members in Europe.

Italy's activity in HRS technology began in 1994 with the purchase and operation of the MIVIS system, a Daedalus whiskbroom sensor, by the CNR. The MIVIS is a passive scanning and imaging instrument that is composed of four spectrometers that simultaneously record reflected and emitted radiation. It has 102 spectral bands from the VIS-NIR-SWIR to the TIR spectral range and the wavelength ranges between 0.43 and 12.7 μm, with an IFOV of 2 mrad and a digitized FOV of 71.1°. The band position was selected to meet research needs that were already known at that time for environmental remote sensing, such as agronomy, archaeology, botany, geology, hydrology, oceanography, pedology, urban planning, atmospheric sciences, and more. Under the Laboratio Aero Per Ricerche Ambientali (LARA) project, the CNR has flown the instrument very intensively since 1994 on-board a

CASA 212 aircraft, acquiring data mostly over Italy and also in cooperation with other nations, such as Germany, France, and the United States (Bianci *et al*. 1996).

In Canada, a new airborne VIS–NIR sensor was developed in 1989 by ITRES (Alberta, Canada), known as CASI. The sensor was a pushbroom programmed sensor aimed at monitoring vegetation and water bodies. ITRES provided data acquisition as well as processing services and also sold a few instruments to individuals who operated the system and then developed measurement protocols for a limited market (e.g., the Free University of Berlin in 1996). In 1996, ITRES developed a research instrument for the Canadian Center for Remote Sensing (CCRS) known as SFSI (Shortwave Infrared Full Spectrum Imager), and recently (2010), they developed an instrument for the LWIR region (8–11.5 μm) named TASI-600 and an instrument for the MWIR region (3–5 μm) named MASI-600 with 64 channels (55 nm bandwidth). The CASI offers several modes, between 512 bands (spectral modes) and 20 preselected bands (spatial modes), with intermediate numbers of spectral bands and pixels being programmable. The spectral range is between 0.4 and 1 μm with a FOV of 29.6° and a IFOV of 2.1 mrad.

The SFSI provides 120 bands (115 used in practice) across the 1.219–2.445 μm spectral region. The FOV is 9.4° and across-track pixels' IFOV is 0.33 mrad. The TASI-600 is a pushbroom thermal imager with 64/32 spectral channels ranging from 8 to 11.5 μm with 600 pixels across track. The FOV is 38°, and the IFOV is 0.49 mrad. The MASI-600 has 64 bands across 3–5 μm with 32 μm bandwidth and a FOV of 40° and an IFOV of 1.2 mrad. ITRES provides to the community also the Shortwave Infrared Airborne Spectral Imager (SASI) sensor operates across the SWIR region (0.950–2.450 μm) with 100 spectral bands at 15 nm sampling interval and 40° FOV. The National Research Council of Canada funded modifications to the SASI sensor to have 160 spectral channels covering the 0.85–2.50 μm spectral range and 38° FOV.

8.5.2
Current HRS Sensors in Europe

Another HRS company, the Finnish Spectral Imaging Ltd. (Specim), has gone quite a long way and can be considered an important benchmark in the HRS arena. From 1995, when the company was founded, they were able to significantly reduce the cost of HRS sensors, making them available to many more users. Two airborne sensors, AISA (airborne image spectrometer for different application)-Eagle and -Hawk for the VIS–NIR and SWIR regions, respectively, were developed, using the PGP (prism-grating-prism) concept invented by Specim in the 1990s. The PGP design enables the construction of a small low-cost spectrometer that is suitable for industrial and research purposes in the wavelength range of 0.32–2.70 μm. Its small size and ease of maintenance and operation, along with the ability to mount the sensor on-board small platforms, have made the Specim sensor accessible to many users who could not otherwise afford to enter the expensive HRS field.

According to Specim, in 2010 more than 70 instruments had been sold worldwide, reflecting the growing interest in this technology in general and in low-cost

capability in particular. This revolution has enabled user independence in terms of data acquisition and operation while providing a breakthrough in HRS strategy in Europe: no longer does one need to count on joint campaigns; the user can plan the mission and the flight, and process the data for his/her particular needs at a relatively low cost. Although the SNR and data performance of the new sensors was not at the level of AVIRIS or HyMAP, the Specim products enabled enlarging HRS capabilities in mission planning, simulation, flight operation, data acquisition, archiving, corrections, calibration, and education. Riding on their success, Specim announced, in 2009, that contracts for a total value of € 1.4 million had been signed with government institutions and private remote sensing companies in Germany, Malaysia, Brazil, and China.

Recent achievements in HRS technology are due, to a certain extent, on the fact that more companies are building and manufacturing small-size HRS sensors for ground and air applications (e.g., HeadWall Photonics: *http://www.headwallphotonics.com/*). While the VIS–NIR sensor is much easier to build, as it is based on available and reliable detectors, the SWIR region is still more problematic.

Two more activities in Europe can be considered important in HRS technology: the first is Instituto Nacional de Tecnica Aeroespacil (INTA) Spain's activity in HRS and the second is the Norwegian company Norsk Elektro Optikk (NEO), which manufactured a new HRS sensor. In 2001, INTA entered the HRS era by first exploring the field and then running a joint venture with Argon ST (a company resulting from a merger between Daedalus Enterprises and S.T. Research Corporation) in 1998, conducting their first campaign in circa 2003 in Southern Spain. The follow-up campaigns demonstrated the HRS concept's promise and, in 2005, the Airborne Hyperspectral Scanner (AHS) was purchased by INTA: it was first operated in Spain and then in other European countries as well. The AHS consisted of 63 bands across the VIS-NIR-SWIR region and 7 bands in the TIR region with a FOV of 90° and IFOV of 2.5 mrad, corresponding to a ground sampling distance (GSD) of 2–7 m. This sensor was flown on-board a CASA 212 aircraft and operated by personnel from INTA. The sensor has been operational in Spain and Europe (via ESA and VITO (Vlaams Instituut Voor Technologisch Onderzoek) since 2005 and remains in good condition until today (2012). The system is well maintained and undergoes a yearly checkup at Argon ST laboratories. Experience gained over the years, along with mechanical upgrading (both electronic and optical), ensures that the sensor will stay operational for a long time.

In about 1995, NEO developed a small HRS satellite sensor (HISS, Hyperspectral Imager for Small Satellites) for ESA, covering the spectral range from 0.4 to 2.5 μm. As ESA did not have any immediate plans for launching such an instrument at the time, the experience gained from the HISS was used to develop a hyperspectral camera for airborne applications – the Applied Spectral Imaging (ASI). The first prototype was built in 1998–1999. In 2001, a collaboration with the Norwegian Defense Research Establishment (FFI) was initiated, which is still continuing today. In the framework of this cooperation, the ASI camera participated in a multinational military measurement campaign in France in 2002. An upgraded

version of the instrument was flown in 2003 and 2004 in different multinational military field trials. In 2004, airborne HRS data were also acquired for several local civilian research institutions. The cooperation with these institutions was continued in 2005 when a further upgraded version of the instrument was flown successfully, including a HRS camera module covering the part of SWIR region (0.9–1.7 μm), in addition to the VIS and NIR regions (0.4–1.0 μm).

All these research activities led to the development of a line of hyperspectral cameras (HySpex) that are well suited for a wide variety of applications in both the civilian and military domains. Main characteristics of the sensor are coverage of the entire range (0.4–2.5 μm) with more than 400 bands with 3.7 and 6.25 nm band width two different sensors (the VNIR 640 and SWIR 320). The sensor underwent several experiments in Europe with proven success but has not yet aggressively entered the commercial remote sensing arena.

Beside the AVIRIS sensor, today the HyMAP sensor has become available: this is a commercially designed and operated system that was based on the Probe-1 sensor (operated in circa 1998 by Applied Signal and Image Technology (ASIT), USA). Several campaigns in the United States demonstrated the promising commercial capability of HRS technology (Kruse *et al.* 2000). Integrated Spectronics, Australia, designed and operated the HyMAP sensor for rapid and efficient wide-area imaging for mineral mapping and environmental monitoring. The sensor can be defined as a high SNR instrument with high spectral resolution, ease of use, a modular design concept, calibrated spectroradiometry, proven in-field operation, and heavy load capacity. It is a whiskbroom sensor with 100–200 bands (usually 126) across the 0.45–2.45 μm spectral region with bandwidths ranging from 10 to 20 nm.

The SNR is in the range of 500 : 1 with 2–10 m spatial resolution. It is characterized by a 60°–70° swath width and furnished with an on-board radiometric and spectral calibration assembly. In 1999, a group shoot using the HyMAP sensor was conducted in the United States. A report by Kruse *et al.* (2000) declared the sensor to be the best available at the time. Since then, the HyMAP sensor has been operated worldwide, providing high-quality HRS data to its end users and opening up a new era in HRS data quality. It has been operated in Europe, Australia, the United States, Asia and Africa in specific campaigns and through Hy Vista activity, which provides end-to-end solutions for the potential customer. HyMAP can thus also be considered a benchmark in HRS technology, which was reached in circa 1999 by Probe-1 and then afterwards by HyMAP sensors. The problem with HyMAP is that the sensor is limited and is operated only by HyVista, and hence, its use is strongly dependent on their schedule and availability. Moreover, the cost of the data is still prohibitive for the daily use capability that is desired from HRS technology. It can be concluded that there is still a significant gap between high SNR and low cost/easy operation in sensors: ideally, this gap might be bridged by fusing the AISA and HyMAP characteristics that are based on two different technologies: pushbroom and whiskbroom, respectively. As more and more companies undertake moving HRS technology forward, we believe that in the near future such a fusion will be possible and we will see more low-cost, high-quality data and more applications emerging from this capability.

In 2011, the APEX has become available to the European research community after a long prototyping and development (Itten *et al.* 2008). It has been built in ESA's Prodex program by Swiss–Belgium collaborative efforts and is operated by VITO, Belgium. This system may be considered a new breakthrough in HRS technology, as it is the first airborne pushbroom system offering a complete coverage of the spectral range between 0.4 and 2.5 μm in one integrated system. APEX provides the same spatial resolution of 1–5 m at 1000 across-track pixels for both the VIS–NIR and SWIR spectral range. The prism design optics allows for very high spectral resolution in the visible part down to 1 nm, whereas the SWIR is resolved with 7 nm. Its data is currently evaluated for various IS applications and the system is to be used for cross-calibration purposes for ESA satellites and alike.

The above provides only the milestone stages in HRS technology over the years. Several of the sensors and activities may not have been mentioned. The reader is therefore directed to a comprehensive description of all HRS sensors until 2008 made by Prof. Gomez from George Mason University in the United States and to a summary of all remote sensing organizations worldwide and all institutes, private sectors, and abbreviations commonly used with this technology at *http://www.tau.ac.il/~rslweb/pdf/HSR.pdf*. A historical list of HRS sensors compiled by Michael Schaepman is available at *http://www.geo.unizh.ch/~schaep/research/apex/is_list.html*.

8.5.3
Satellite HRS Sensors

Among the airborne HRS benchmarks mentioned earlier, orbital HRS activity has contributed greatly to the blossoming HRS activity. The first initiative to place an HRS sensor in orbit took place in the early 1990s when a group of scientists chaired by Goetz started work on the NASA HRS mission HIRIS (High Resolution Imaging Spectrometer). This was part of NASA's High-Resolution Imaging Spectrometer Earth Observation System program. The idea was to place an AVIRIS-like sensor in orbit with a full range between 0.4 and 2.5 μm and a spatial resolution of 30 m. A report that provides the capacity of this sensor, including its technical and application characteristics, was issued in several copies (Goetz, 1987). This report was the first document that showed the intention to go into space with HRS. The HIRIS mission was terminated, apparently because of the Challenger space shuttle disaster, which significantly changed the space programs at NASA.

The scientists, however, agreed that using HRS in orbit is an important task that needs to be addressed (Nieke *et al.* 1997). A report by Hlao and Wong (2000) submitted to the US Air Force in 2000 assessed the technology as premature and still lagging behind other remote sensing technologies such as air photography. The next benchmark in orbital HRS was Hyperion, part of the NASA New Millennium Program (NMP). The Hyperion instrument was built by TRW Inc.

(Thompson Ramo Woddbridge) using focal planes and associated electronics remaining from the Lewis spacecraft, a product of the NASA Small Satellite Technology Initiative (SSTI) mission that fell in 1997. The integration of Hyperion took less than 12 months from Lewis's spare parts and was sent into orbit on-board the EO-1 spacecraft. The mission, planned for 3 years, is still operational today (2012) with a healthy sensor and data, although the SNR is poor. The instrument covers the VIS-NIR-SWIR region from 0.422 to 2.395 μm with two detectors and 244 bands of 10 nm bandwidth. The ground coverage FOV provided a 7.5 km swath and 30 m GSD. The first data sets cost around US$2500 and had a lower SNR than originally planned. Nonetheless, over the years, and despite its low quality, the instrument has brought new capability to sensing the globe by temporal HRS coverage, justifying the effort to place a better HRS sensor in space. As of the summer of 2009, Hyperion data are free of charge, which has opened up a new era for potential users. In circa 2001, the CHRIS (Compact High Resolution Imaging Spectrometer) sensor was launched into orbit on-board the PROBA (Project on Board Autonomy) bus. It was developed by the Sira Electro Optic group and supported by the ESA. The CHRIS sensor is a high spatial resolution hyperspectral spectrometer (18 m at nadir) with a FOV resulting in 14 km swath.

One of its most important characteristics is the possibility of observing every ground pixel at the same time, in five different viewing geometry sets (nadir, $\pm 55^{\circ}$ and $\pm 36^{\circ}$). It is sensitive to the VIS–NIR region (0.41–1.059 μm), and the number of bands is programmable, with up to 63 spectral bands. Although limited in its spectral region, the instrument provides a first view of the bidirectional reflectance distribution function (BRDF) effects for vegetation and water applications, and it is robust, as it is still operating today. The ''early'' spaceborne planning missions in both the United States and Europe comprised, among others, the following projects: IRIS (Interface Region Imagery Spectrograph), HIRIS (NASA), GEROS (German Earth Resources Observer System, USA), HERO (Hyperspectral Environmental and Resource Observer, CSA), PRISM (Process Research by an Imaging Space Mission), SPECTRA (Surface Processes and Ecosystem Changes Through Response Analysis, all ESA), SIMSA (Spectral Imaging Mission for Science) and SAND (Spectral Analysis of Dryland). Although most of these initiatives were not further funded and are not active today, they demonstrated government agencies' interest in investing in this technology, albeit with a fearful and cautious attitude. Other orbital sensors, such as MODIS (Moderate Resolution Imaging Spectrometer), MERIS (Medium Resolution Imaging Spectrometer), and ASTER (Advanced Spaceborne Thermal Emission and Reflection), can also be considered part of the HRS activities in space, but in terms of both spatial (MODIS and MERIS) and spectral (ASTER) resolution, these sensors and projects still lag behind the ideal HRS sensor that we would like to see in orbit with high spectral (more than 100 narrow bands) and spatial (less than 30 m) resolutions. It is important to mention, however, that a new initiative to study the moon and Mars using HRS technology took place by a collaboration between NASA and ISA (India), within which the M^3 mission to the moon has recently provided

remarkable results by mapping a thin layer of water on the moon's surface (Pieters *et al.* 2009b,a). In addition, missions to Mars, such as CRISM (Compact Reconnaissance Imaging Spectrometer for Mars) show that it is now understood that HRS technology can provide remarkable information about materials and objects remotely.

EnMAP is a German hyperspectral satellite mission providing high-quality hyperspectral image data on a timely and frequent basis. Its main objective is to investigate a wide range of ecosystem parameters encompassing agriculture, forestry, soil and geological environments, coastal zones, and inland waters. This will significantly increase our understanding of coupled biospheric and exospheric processes, thereby enabling the management and guaranteed sustainability of our vital resources. Launch of the EnMAP satellite is envisaged for 2015 (updated in 2012). The basic working principle is that of a pushbroom sensor, which covers a swath (across-track) width of 30 km, with a GSD of 30×30 m. The second dimension is given by the along-track movement and corresponds to about 4.4 ms exposure time. This leads to a detector frame rate of 230 Hz, which is a performance-driving parameter for the detectors, as well as for the instrument control unit and the mass memory. HyspIRI is a new NASA initiative to place a HRS sensor in orbit and is aimed at complementing EnMAP, as its data acquisition covers the globe periodically.

It is important to mention that other national agencies are aiming to place HRS sensor in orbit as well. A good example is PRISMA of the Italy's space agency. PRISMA is a pushbroom sensor with swath of 30–60 km, GSD of 20–30 m (2.5–5 m peroxyacetylnitrate (PAN)) with a spectral range of 0.4–2.5 μm. The satellite launch was foreseen by the end of 2013, but it seems that some delay is encountered and the new lunch date is unknown.

To keep everyone up to date and oriented on the efforts being made in HRS pace activities, a volunteer group was founded in November 2007 by Dr Held and Dr Staenz named ISIS (International Satellite Imaging Spectrometry) (Staenz, 2009). The ISIS group provides a forum for technical and programming discussions and consultation among national space agencies, research institutions, and other spaceborne HRS data providers. The main goals of the group are to share information on current and future hyperspectral spaceborne missions and to seek opportunities for new international partnerships to the benefit of the global user community. The initial ''ISIS Working Group'' was established following the realization that there were a large number of countries planning HRS (''hyperspectral'') satellite missions with little mutual understanding or coordination. Meetings of the working group have been held in Hawaii (IGARSS 2007), Boston (IGARSS 2008), Tel Aviv (EARSeL 2009), Hawaii (IGARSS 2010), Vancouver (IGARSS 2011) and Munich (IGARSS 2012). The technical presentations by the ISIS group have garnered interest from space agencies and governmental and industrial sectors in this promising technology. An excellent review on current and planned civilian space hyperspectral sensor for Earth observation (EO) is given by Buckingham and Staenz (2008).

8.6 Potential and Applications

Merging of spectral and spatial information, as is done within HRS technology, provides an innovative way of studying many spatial phenomena at various resolutions. If the data are of high quality, they allow near-laboratory level spectral sensing of targets from afar. Thus, the information and knowledge gathered in the laboratory domain can be used to process the HRS data on a pixel-by-pixel basis. The ''spheres'' that can feasibly be assessed by HRS technology are atmosphere, pedosphere, lithosphere, biosphere, hydrosphere, and cryosphere. Different methods of analyzing the spectral information in the HRS data are known, the basic one consisting of comparing the pixel spectrum with a set of spectra taken from a well-known spectral library. This allows the user to identify specific substances, such as minerals, chlorophyll, dissolved organics, atmospheric constituents, and specific environmental contaminants, before moving ahead with other more sophisticated approaches (Section 8.8.4). The emergence of hyperspectral imaging moved general remote sensing applications from the area of basic landscape classification into the realm of full spectral quantification and analysis. The same type of spectroscopy applications that have been utilized for decades by chemists and astronomers are now accessible through both nadir and oblique viewing applications. The spectral information enables the detection of indirect processes, such as contaminant release, based on changes in spectral reflectance of the vegetation or leaves. The potential thus lies in the spectral recognition of targets using their spectral signature as a footprint and on the spectral analysis of specific absorption features that enable a quantitative assessment of the matter in question. Although many applications remain to be developed, within the past decade, significant advances have been made in the development of applications using hyperspectral data, mainly because of the extensive availability of today's airborne sensors. While, a decade ago, only a few sensors were available and used in the occasional campaign, today, many small and user-friendly HRS sensors that can operate on any light aircraft are available.

Hydrology, disaster management, urban mapping, atmospheric study, geology, forestry, snow and ice, soil, environment, ecology, agriculture, fisheries, and oceans and national security are only a few of the applications for HRS technology today. In 2001, van der Meer and Jong (2001) published a book with several innovative applications for that time. Since then, new applications have emerged and the potential of HRS has been discussed and analyzed by many authors at conferences, in proceedings papers and full-length publications. In a recent paper, Staenz (2009) provides his present and future notes on HRS, which very accurately summarize the technology up to today. In the following, we paraphrase and sharpen Staenz's points. It is clear from the numerous studies that have been carried out that HRS technology has significantly advanced the use of remote sensing in different applications (e.g., AVIRIS 2007). In particular, the ability to extract quantitative information has made HRS a unique remote sensing tool. For example, this technology has been used by the mining industry for exploration of natural resources, such as the identification

and mapping of the abundance of specific minerals. HRS is also recognized as a tool to successfully carry out ecosystem monitoring, especially the mapping of changes because of human activity and climate variability. This technology also plays an important role in the monitoring of coastal and inland waters. Other capabilities include the forecasting of natural hazards, such as mapping the variability of soil properties that can be linked to landslide events, and monitoring environmental disturbances, such as resource exploitation, forest fires, insect damage, and slope instability in combination with heavy rainfall. As already mentioned, HRS can be used to assess quantitative information about the atmosphere such as water vapor content; aerosol load; and methane, carbon dioxide, and oxygen content. HRS can also be used to map snow parameters, which are important in characterizing a snow pack and its effect on water runoff. Moreover, the technology has shown potential for use in national security, for example, in surveillance and target identification, verification of treaty compliance (e.g., Kyoto Accord on Greenhouse Gas Emission), and disaster preparedness and monitoring (Staenz, 2009). Some recent examples show both the quantitative and exclusive power of HRS technology in detection of soil contamination (Kemper and Sommer, 2003), soil salinity (Ben-Dor *et al*. 2002), species of vegetation (Ustin *et al*. 2008), atmospheric electromagnetic emissions of methane (Noomem, Meer, and Skidmore, 2005), detection of ammonium (Gersman *et al*. 2008), asphalt condition (Herold *et al*. 2008), water quality (Dekker *et al*. 2001), and urban mapping (Ben-Dor, 2001). Many other applications can be found in the literature and still others are in the R&D phase in the emerging HRS community. Nonetheless, although promising, one should remember that HRS technology still suffers from some difficulties and limitations. For example, the large amount of data produced by the HRS sensors hinders this technology's usefulness for geometry analysis or visual cognition (e.g., building structures and roads) and one has to weight the added value promised by the technology for one's applications. There are other remote sensing tools and the user should consult with an expert before using HRS technology. Since the emergence of HRS, many technical difficulties have been overcome in areas such as sensor development, data handling, aviation and positioning, and data processing and mining. However, there are several main issues that require solutions to move this technology toward more frequent operational use today. These include a lack of reliable data sources with a high SNR are required to retrieve the desired information and temporal coverage of the region of interest; although analytical tools are now readily available, there is a lack of robust automated procedures to process data quickly with a minimum of user intervention; the lack of operational products is obviously due to the fact that most efforts to date have been devoted to the scientific development of HRS; interactions with other HRS communities have not yet developed – there are many applications, methods, and know-how in the laboratory-based HRS disciplines but no valid connection between the communities; systems that can archive and handle large amounts of data and openly share the information with the public are still lacking; only a thin layer of the surface can be sensed; there is no standardization for data quality or quality indicators (QI); not much valid experience exists in merging HRS data with that

of other sensors (e.g., LIDAR, SAR (Synthetic Aperture RADAR)); many sensors have emerged in the market but their exact operational mechanism is unknown, biasing an accurate assessment; thermal HRS sensors are just starting to emerge, whereas point thermal spectrometers are existing (Christensen *et al*. 2000); oblique view and ground-based HRS measurements have not yet been frequently used; the cost of deriving the information product is too high, since the analysis of HRS data is currently too labor intensive (not yet automated); it is not yet recognized by potential users as a routine vehicle as, for example, is air photography; not too many experts in this technology are available. Several authors have summarized this technology's potential to learn from history, such as Itten (2007); Schaepman *et al*. (2009) and Staenz (2009).

It is anticipated that HRS technology will catch up when new high-quality sensors are placed in orbit and the data become available to all (preferably in reflectance values), when the air photography industry uses the HRS data commercially, and when new sensors that are inexpensive and easy to use are developed along with inexpensive aviation (such as unmanned aerial vehicle, UAV).

8.7 Planning of an HRS Mission

In this section, we describe major issues for the planning of a mission for an airborne campaign: we do not cover the possible activities involved for a spaceborne mission. Planning a mission is a task that requires significant preparation and knowledge of the advantages and disadvantages of the technology. The idea behind using HRS is to get an advanced thematic map as the final product which no other technology can provide. In the planner's mind, the major step toward achieving the main prerequisite of a thematic map is to generate a reflectance or emission image from the raw data.

First, a scientific (or applicable) question has to be asked, such as Where can saline soil spots be found over a large area? For such a mission, the user has to determine whether there exists spectral information on the topic which is being covered by the current HRS sensor. This investigation might consist of self-examination or a literature search of both the area in question and the advantageous of using HRS (many times, HRS is an overkill technology for answering simple thematic questions). Once this investigation is carried out, the question is What are the exact spectral regions that are important for the phenomenon in question and what pixel size is needed? In addition, the question of what SNR values will enable such detection should be raised. Having this information in hand, the next step is to search for the instrument. Sometimes, a particular instrument is available, and there is no other choice. In this case, the first spectral investigation stage should focus on the available HRS sensor and its spectral performances (configuration, resolution, SNR, etc.) infrastructure. It is recommended that the spectral information on the thematic question be checked at the sensor-configuration

stage. In some sensors, especially pushbroom ones, it is possible to program the spectral configuration using a new arrangement of the CCD assembly.

In this respect, it is important that the flight altitude be taken into consideration (for both pixel size and integration time) along with aircraft speed. Most sensors have tables listing these components and the user can use them to plan the mission frame. As within this issue, the user can configure the bands with different FWHM and positions; it should be remembered that combined with spatial resolution, this might affect the SNR. When selecting the sensor, it is important to obtain (if this is the first use) a sample cube to learn about the sensor's performance. It is also good to consult with other people who have used this equipment. Getting information on when and where the last radiometric calibration was performed as well as obtaining information about the sensor stability and uncertainties is very important. It is better if the calibration file of the sensor is provided but if not, the HRS owner should be asked for the last calibration date and its temporal performances.

Quality assurance (QA) of the sensor's radiance must be performed in order to assure a smooth step to the next stage, namely, atmospheric correction. Methods and tools to inspect these parameters were developed under EUFAR JRA2 initiative and recently also by Brook and Ben-Dor (2011).

The area in question is generally covered by 30% overlap between the lines. This has to be carefully planned in advance taking into consideration the swath of the sensor and other aircraft information (e.g., stability, time in the air, speed and altitude preferences, navigation systems). A preference for flying toward or against the direction of the Sun's azimuth needs to be decided on, and it is recommended that the Google Earth interface be used to allocate the flight lines and to provide a table for each line with starting and ending points for all flight lines. One also needs to check if the GPS is available and configure the system to be able to ultimately allocate this information in a readable and synchronized form.

A list of go/no go items should be established. For instance, a forecast for the weather should be on hand 24 h in advance, with updates every 3 h. If possible, a representative should be sent to the area in question to report on cloud coverage close to acquisition time. In our experience, one should be aware of the fact that a 1/2 cover over the area in question will turn into almost 100% coverage of the flight lines that appeared to be free of clouds. Moreover, problems that may emerge at the airport need to be taken into consideration, such as the GPS is not functioning or the altitude obtained from air control is different from that which was planned. The go/no go checklist should be used for these issues as needed. Each go/no go list is individual, and one should be established for every mission.

The aircrew members (operators, navigator, and pilot) must be briefed before and debriefed after the mission. A logbook document should be prepared for the aircrew members (pilot and operator) with every flight line reported by them. It is important to plan a dark current acquisition before and after each line acquisition. Acquisition of a vicarious calibration site (in the area of interest or on the way to this area) in question should also be planned for, that is well prepared and documented in advance. If possible, radio contact with the aircrew should be obtained at a

working frequency before, during, and after the overpass. A ground team should be prepared and sent to the area in question for the following issues: (i) calibrating the sensor's radiance and examining its performance (Brook and Ben-Dor, 2011), (ii) validating the atmospheric correction procedure, and (iii) collecting spectral information that will be useful further on for thematic mapping (e.g., chlorophyll concentration in the leaves). The ground team should be prepared according to a standard protocol, and it should be assured that they are furnished with the necessary equipment (such as video and still cameras, field spectrometer, maps, Sun photometer, and GPS). After data acquisition both from air and ground, the data should be immediately backed up and quality control checks run to determine data reliability. Afterward, the pilot logbook, ground documentation, and any other material that evolved during the mission should be collected.

In general and to sum up the above, a mission has to be lead by a senior person who is responsible to coalesce the end user needs, the ground team work, the airborne crew activity, and the processing stages performed by experts. He/she is responsible to interview the end user and understand the question at hand and is responsible to allocate a sensor for the mission and meet with the sensor owner and operator ahead of the mission and arrange a field campaign by a ground team. Other responsibilities such as arranging logistics and briefing of all teams as well as backing up the information just after the mission end, that is, at the airport are also part of their duties and are very important. A checklist and documents on every stage are available in many bodies (e.g., DLR, TAU, the Tel Aviv University), but in general, it can be developed by any group by gathering information from main HSR leading bodies (DLR, NASA, INTA).

8.8 Spectrally Based Information

A remotely sensed object interacts with electromagnetic radiation where photons are absorbed or emitted via several processes. On the Earth's surface (solid and liquid) and in its atmosphere (gasses and aerosol particles), the interaction across the UV-VIS-NIR-SWIR-TIR regions is sensed by HRS means to give additional spectral information relative to the common multiband sensors. The spectral response of the electromagnetic interaction with matter can be displayed as radiance, reflectance, transmittance, or emittance, depending on the measurement technique and the illumination source used. Where interactions occur, a spectrum shape can be used as a footprint to assess and identify the matter in question. Variations in the position of local minima (or maxima, termed ''peaks'') and baseline slope and shape are the main indicators used to derive quantitative information on the sensed material. The substance (chemical or physical) that significantly affects the shape and nature of the target's spectrum is termed ''chromophore.'' A chromophore that is active in energy absorptance (e.g., chlorophyll molecule in vegetation) or emission (e.g., fluorescence) at a discrete wavelength is termed a ''chemical chromophore.'' A chromophore that governs the spectrum's shape (such as the slope and albedo

Table 8.2 A summary of possible chromophores in all spheres of interest for our planet by remote sensing using the spectral information available on the Earth surface.

Sphere	Pedosphere	Lithosphere	Biosphere	Hydrosphere	Cryosphere	Atmosphere
0.35–1 μm VIS–NIR						
Abs-electronic	Fe, Ni+	Fe, Ni+	Chloro-phyll+	Chloro-phyll+		
Scattering particles	Particle size	Particle size	Leaf structure	Particle size	Particle size	Mie, Rayleigh
Emission - electronic	—	—	Fluorescence	—	—	
Abs-overtones	—	OH- 3 ν Overtone	H_2O	H_2O	—	O_2, H_2O, O_3, NO_2
1–2.5 μm SWIR						
Abs-electronic						
Scattering particles	Albedo-particle size	Albedo-particle size	Leaf structure	—	Particle	Mie
Emission–electronic	—	—	—	—	—	—
Abs-Overtones combination modes	OH, C−H, N−H+	+	+	H_2O	H_2O	H_2O, CO_2, O_2, CH_4
3–12.5 μm MWIR–LWIR						
Abs-electronic	—	—	—	—	—	—
Scattering particles	—	—	—	—	—	Mie
Emission–electronics	Temperature	Temperature	Temperature	Temperature	Temperature	—
Abs Fundamentals	Emissivity, SI−O, Al−O, Fe−O	Emissivity, SI−O, Al−O, Fe−O	Emissivity C=O	Emissivity H_2O, OM	Emissivity	SO_4 NH_3 CO_2

+, some other causes for the spectral mechanism visualization.

(e.g., particle size, refraction index)) is termed ''physical chromophore.'' Often, the spectral signals related to a given chromophore overlap with the signals of other chromophores, thereby hindering the assessment of a specific chromophore. The spectrum of a given sample, which is the result of all chromophore interactions, can be used to analyze and identify the matter if a spectral-based method for that end spectrum is used. Fourier and other spectral tools (e.g., wavelet transforms, principle component analysis) that are usually applied to laboratory spectra can be

excellent tools for application to HRS data provided the data are of good quality. A comprehensive review of chemical and physical chromophores in soils and rocks, as an example, can be found in Irons, Weismiller, and Petersen (1989); Ben-Dor, Irons, and Epema (1999); Clark (1999); Malley, Martin, and Ben-Dor (2004); McBratney and Rossel (2006). A compilation table that provides the chromophores of known Earth targets in all spheres is given in Table 8.2. The table, which covers all spectral regions (VIS, NIR, SWIR, MWIR, and LWIR), may be of interest for HRS technology from field, air, and space levels.

The chemical chromophores in the VIS-NIR-SWIR regions refer to two basic chemical mechanisms: (i) overtones and combination modes in the NIR–SWIR region that emerge from the fundamental vibrations in the TIR regions and (ii) electron processes in the VIS region that are in most cases crystal-field and charge-transfer effects. The physical chromophores in this region refer mostly to particle size distribution and to refraction indices of the matter in question. The electronic processes are typically affected by the presence of transition metals, such as iron, and although smeared, they can be used as a diagnostic feature for iron minerals (around 0.80–0.90 μm crystal field and around 0.60–0.70 μm charge transfer).

Accordingly, all features in the UV-VIS-NIR-SWIR-TIR spectral regions have a clearly identifiable physical basis. In solid–fluid Earth materials, three major chemical chromophores can be roughly categorized as follows: (i) minerals (mostly clay, iron oxide, primary minerals-feldspar, Si, insoluble salt, and hard-to-dissolve substances such as carbonates, and phosphates), (ii) organic matter (living and decomposing), and (iii) water (solid, liquid, and gas phases). In gaseous Earth materials, the two main chemical chromophores are (i) gas molecules and (ii) aerosol particles of minerals, organic matter, and ice.

Figure 8.3 presents a summary of possible chromophores in soils and rocks (Ben-Dor, Irons, and Epema, 1999). Basically, the (passive) electromagnetic sources for HRS are the radiation of Sun and Earth (terrestrial) (Sun: VIS-NIR-SWIR, Sun and Earth: TIR). Assuming that in a photon pack emitted from a given source (F; F_0 for Sun, F_e for Earth), some photons may be absorbed (F_α), reflected (F_ρ), or transmitted (F_τ) at a given wavelength and incident angle. The energy balance (in terms of flux densities) on a given target for every boundary (atmosphere, geosphere, and hydrosphere) can be written as follows:

$$F = F_\tau + F_\alpha + F_\rho \tag{8.1}$$

where $F = F_0 + F_e$ or any other incident light hitting the target (e.g., F_g, F_{wf}, and F_{ws} for ground, water floor, and water surface, respectively; Figure 8.4a,b). If we assume that we know the source energy (e.g., F_0), dividing Eq. (8.1) by F_0 gives

$$1 = \tau + \alpha + \rho \tag{8.2}$$

where τ is the transmittance, α the absorptance, and ρ the reflectance coefficients, respectively. These coefficients describe the proportion of F_τ, F_α, and F_ρ, respectively and range from 0 to 1. In an ideal cases, the Sun emits photons (F_0) that pass through the atmosphere and hit the ground (F_g) and then are reflected back

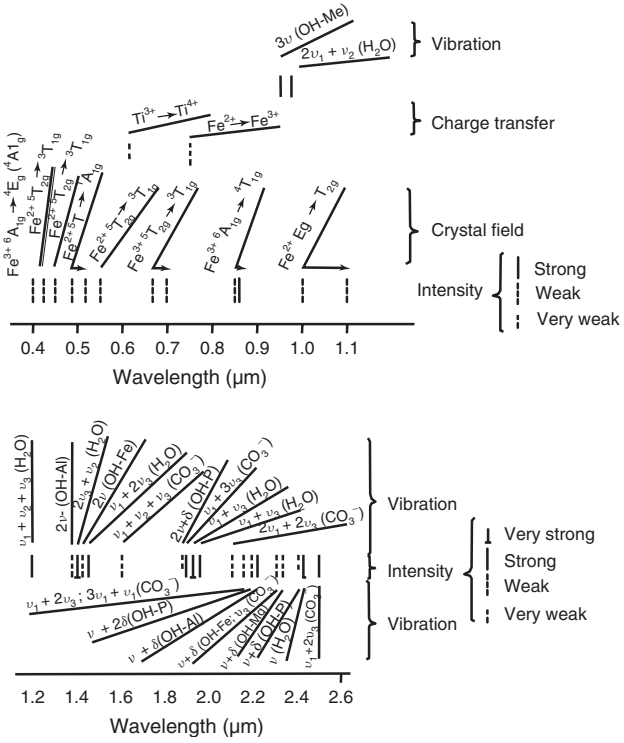

Figure 8.3 Compilation of chromophores in soil and rocks: VIS–NIR electronic processes and overtones, SWIR overtones and combination modes. (Source: Taken from Ben-Dor, Irons, and Epema (1999).)

to the sensor. Figure 8.4 provides a schematic view of two targets (solid and water) and three mediums (atmosphere, geosphere, and hydrosphere). This schematic illustration shows an ideal case demonstrating the role of each coefficient at every sphere. Across the spectral range where the atmosphere is (semi) transparent to the photons (known as *atmospheric window*) or where the atmospheric attenuation is modeled, the atmospheric transmittance (τ_a) and reflectance (ρ_a, term scattering) change based on the atmospheric condition. Accordingly, it is possible to estimate the atmospheric absorptance (α_a) if both τ_a and ρ_a are known; Eq. (8.2) can be written as

$$1 = \tau_a + \alpha_a + \rho_a \tag{8.3}$$

where τ_a and ρ_a are measured or estimated by radiative transfer models (or local measurements), enabling extracting of the atmosphere absorptance (α_a) as well as to provide the new energy flux densities that hit the ground surface (F_g, irradiance).

F_g serves afterwards as an energy source for the geosphere and hydrosphere interactions with the electromagnetic radiation. Figure 8.4a illustrates the interaction of F_g with the Earth's solid surface (geosphere) and Figure 8.4b presents the

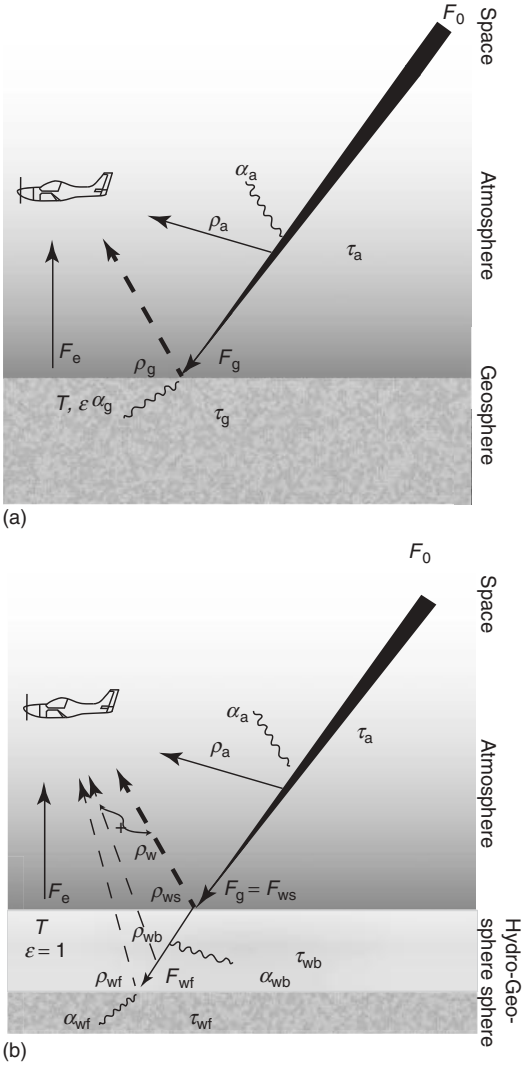

Figure 8.4 Schematic views of two and three mediums (atmosphere and geosphere (a) and atmosphere, hydrosphere, and geosphere (water floor surface) (b), respectively). The following symbols are used: F_0, emission by the Sun (Planck); F_e, Earth emission (Planck); T, Earth temperature; ϵ, emissivity; τ_a, transmittance of atmosphere; α_a, absorptance of atmosphere; ρ_a, reflectance of atmosphere; τ_g, transmittance of solid Earth surface (ground); α_g, absorptance of solid Earth surface (ground); ρ_g, reflectance of the solid Earth surface (ground); τ_{wb}, transmittance of water body; α_{wb}, absorptance of water body; ρ_{wb}, reflectance of water body; ρ_{ws}, reflectance of water surface; ρ_{wf}, reflectance of water floor surface; τ_{wf}, transmittance of water floor surface; α_{wf}, absorptance of water floor surface; F_{ws}, irradiance at surface level; and F_{wf}, irradiance at sea floor level.

interaction with a water body (hydrosphere). In the first example (Figure 8.4a – geosphere), the surface is considered to be opaque and thus the transmittance (τ_g) is set to zero. Accordingly, Eq. (8.2) for the geosphere becomes

$$1 = \alpha_g + \rho_g \tag{8.4}$$

As α_g reflects the material's chemical and physical properties, its extraction can be made by measuring the surface reflectance ρ_g only. Accordingly, this procedure (to extract the surface reflectance) is a key issue in the HSR arena. In the second example (Figure 8.4b, hydrosphere), the water surface is not opaque and thus F_g (also F_{ws}) is divided between direct and indirect portions of photons: those which are reflected from the water to the atmosphere (expressed as reflectance coefficient of the water surface (ρ_{ws}) and those which are scattered from the water body back (expressed as the water body reflectance ρ_{wb}), respectively:

$$\rho_w = \rho_{ws} + \rho_{wb} \tag{8.5}$$

Also, transmittance photons penetrate into the water medium (expressed by the coefficient of transmittance (τ_{wb}), whereas some photons are absorbed by the water body (expressed by the coefficient of absorptance; α_{wb}). As all of the coefficients in this cases are greater than zero, Eq. (8.3) can be written as

$$1 = \tau_{wb} + \alpha_{wb} + (\rho_{ws} + \rho_{wb}) \tag{8.6}$$

As ρ_w depends on the water condition, it is likely that in shallow clean water, where $\rho_{ws} + \rho_{wb} \to 0$, there will be enough photons to penetrate the water body and hit the water floor surface (F_{wf}). This energy (F_{wf}) is then reflected back to the water volume depending on the water floor surface characteristics. In this case, the water floor can be considered opaque (part of the geosphere), leading to $\tau_{wf} = 0$. Accordingly, Eq. (8.2) for the water floor becomes

$$1 = \alpha_{wf} + \rho_{wf} \tag{8.7}$$

where α_{wf} is the water floor absorptance and ρ_{wf} the water floor reflectance. The radiance acquired on-board an HSR sensor is a product of the Sun irradiation (F_0) that is attenuated by all the above mentioned processes (reflectance, absorptance, and transmittance) and their corresponding coefficients. As previously discussed, the absorptance is the most important coefficient for the diagnosis of each sphere since it relates to the chemical and physical properties of the sensed matter. Doing so spectrally can discriminate between the chemical compound being in the atmosphere, geosphere, and hydrosphere. In each sphere, different ways to extract α are taken. To estimate α for the geosphere case, only one degree of freedom is valid in Eq. (8.4) and thus acquiring the reflectance (ρ_g) is an easy task. In the case of atmosphere and hydrosphere, the estimation of the absorptance α is more complicated as two degrees of freedom in Eqs. (8.5) and (8.6) exist (ρ_a, ρ_{wb}, τ_a, and τ_{wb}). This makes the analysis in this case more complicated. In general, all coefficients are playing an important role in order to recover the at-sensor radiance; a full solution to extract ρ_g, $\rho_a + \tau_a$, and ρ_{wf} from the at-sensor radiance is further discussed in the atmospheric removal section (Section 8.9.2).

It is important to mention that all the previous discussion is schematic in order to illustrate how energy decays from the sun to the sensor while interacting with several materials in each sphere. This also highlights how some of the coefficients are important for the HSR concept (e.g., extracting reflectances for the geosphere). No consideration to BRDF, topography, and adjacency effects were taken in this discussion.

The original source of energy (F_0, F_e) can be calculated (or measured) according to Planck's displacement law of a black body entity (depending on its temperature). This calculation shows that the radiant frequencies are different using the Sun (VIS-NIR-SWIR) or Earth (TIR) and thus demonstrates separate HRS approaches using the Sun (mostly performed) and the Earth (just emerging) as radiation sources. When the Sun serves as the radiant source, the reflectance of the surface ρ_g is used as a diagnostic parameter to map the environment. When the Earth serves as the radiant source, the emissivity (ϵ) and the temperature (T) are used as diagnostic parameters. These parameters can be derived from the acquired radiances using several methods to remove atmospheric attenuation (mostly τ_a, and then after separating between T and ϵ (in the TIR region) or extracting ρ_g (in the VIS-NIR-SWIR region)). The reflectance and emissivity are inherent properties of the sensed matter that do not change with external conditions (e.g., illumination or environmental conditions) and hence are used as diagnostic parameters. They both provide, if high spectral resolution is used, spectral information about the chromophores within the matter being studied.

According to Kirchhoff's law, the absorptivity of a perfect black body material is equal to its emissivity (in equilibrium) and thus reflectance has a strong relation to emissivity across the spectral region studied, that is, $\epsilon = 1 - \rho_g$. In atmospheric windows where $\tau \neq 0$ across the VIS-NIR-SWIR-MWIR and LWIR region, HRS can be performed using atmospheric correction techniques as shown in Figure 8.5. While the LWIR (8–12 μm) is sufficient for remote sensing of the Earth (if the temperature is known), as is the VIS-NIR-SWIR region, the MWIR (3–5 μm) region is more problematic for HRS remote sensing of the Earth, as both Sun and Earth Planck functions provide low radiation in their natural position (Sun 6000 K, Earth 300 K) and overlap across this region. Hence, the MWIR region across 3–5 μm is usable for hot (Earth) targets that enable the dominant photons to be above the Sun's background across this region. It should be noted that ρ_g and α_g are important parameters for assessing the Earth's surface composition, but if they are known in advance (e.g., ground targets with known ρ_g), τ_a and α_a can be extracted at specific wavelengths and hence can provide information about the atmospheric constituents (gases and aerosol particles). In other words, HRS can also be a tool to quantitatively study the atmosphere.

While in the VIS region, only limited information on terrestrial systems is available, important information about many of the Earth's materials can be extracted from the NIR–SWIR region. This is because in the VIS region, the electronic processes responsible for broad spectral features are dominant, whereas in the NIR–SWIR region, overtone and combination modes of fundamental vibrations responsible for noticeable spectral features are dominant. Many of

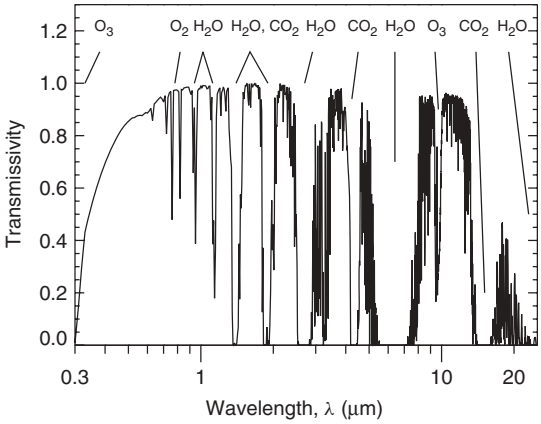

Figure 8.5 Spectral distribution of simulated solar atmospheric transmissivity. Absorption bands correspond to O_3: $< 0.3\,\mu m$; $9.6\,\mu m$; O_2: $0.76\,\mu m$; H_2O: 0.72, 0.82, 0.94, 1.1, 1.38, 1.87, and $2.7\,\mu m$; $6.3\,\mu m$; CO_2: 1.4, 2.0, and $2.7\,\mu m$; $4.3, 15\,\mu m$. The simulations were performed with MODTRAN4 (Version 3 Revision 1, MOD4v3r1) with the Sun in the zenith, the spectral results were averaged over a FWHM of 10 nm. (Source: Adapted from Wendisch and Yang (2012).)

the Earth's materials show significant spectral absorption in the NIR–SWIR region, which serves as a unique fingerprint for mineral identification (Hunt and Salisbury, 1970,1971; Hunt, Salisbury, and Lenhoff, 1971a,b). In addition, atmospheric gases, such as oxygen, water vapor, carbon dioxide, and methane, produce specific absorption features in the VIS-NIR-SWIR regions (Goetz, 1991). Lying in the narrow band's width (usually more than 10 nm) that HRS is capable of generating are spatial qualitative and quantitative indicators for ecologists, land managers, pedologists, geologists, limnologists, atmospheric scientists, and engineers, for which the selection of appropriate methods is dependent on the particular management objectives and the characteristics of the indicators.

In general, the above mentioned spectral information is part of the radiance at sensor, among other factors (such as sun angle, viewing angle, terrain relief, and atmosphere attenuation). To extract the spectral information that are considered inherent properties of the sensed matter, a special data analysis stage must be applied.

8.9 Data Analysis

8.9.1 General

Data processing is performed following a chain procedure, an example of which is given in Figure 8.6. It starts with quality assessment (and assurance, QA) of the raw data and data preprocessing to obtain reliable radiance information and later,

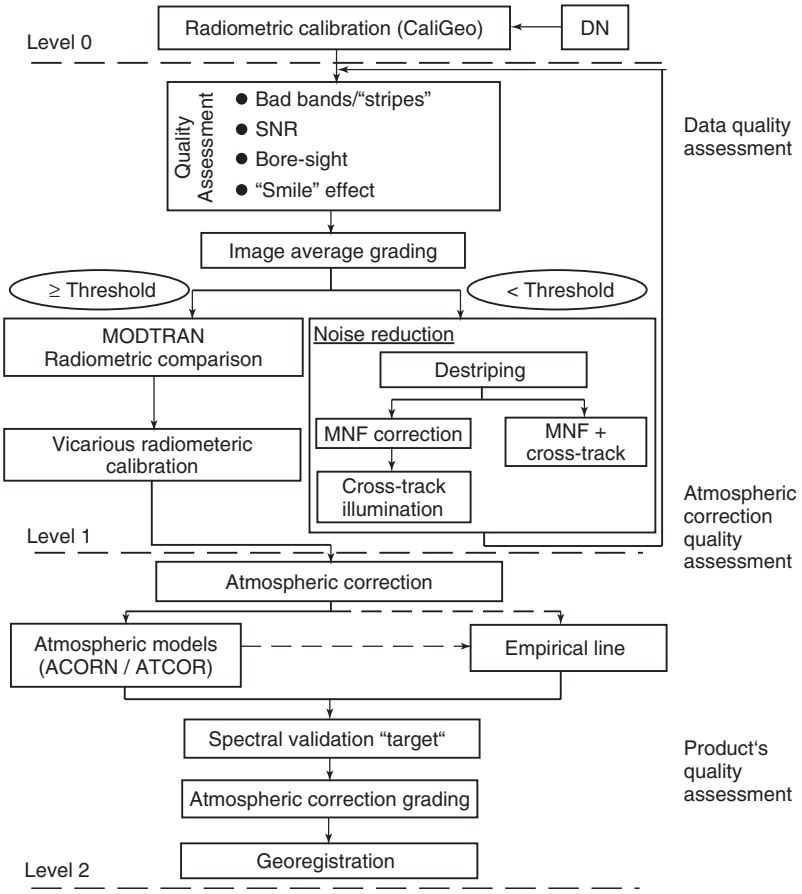

Figure 8.6 A data-processing chain, as used at RSL-TAU (Remote Sensing Laboratory at the Tel Aviv University) with the AISA-Dual sensor. Note that at three stages, quality assurance is crucial: the raw data (including radiance), the atmospheric correction stage (reflectance and emittance), and the thematic mapping stage.

a final product (thematic maps). For each stage, QI are used (denotes ''grading'' in Figure 8.6). Then, the data should undergo atmospheric correction to yield reliable reflectance (or emittance) data. The cube is then transferred to the ''thematic processing'' stage in which background knowledge (supervised classification) or the absence of information (unsupervised classification) are used.

8.9.2 Atmospheric Correction

As most of the HRS sensors are operating across the VIS-NIR-SWIR region, the current section deals with atmosphere correction in this wavelength region. The results are either directional surface reflectance quantities or the spectral albedo

values (Nicodemus *et al*. 1977). Note, we use the term ''reflectance'' hereafter as a generic term of a relation between reflected and incoming radiative flux (Eq. (8.2)). This radiometric conversion of the measured radiance to reflectance is referred to as ''atmospheric correction'' already in early remote sensing literature (Dozier and Frew, 1981). Note that the term ''correction'' is appropriate as long as data are adjusted to match a given ground reference by empirical methods. However, it may be misleading for methods relying on physical radiative transfer models. The term ''atmospheric compensation'' would be a more appropriate description in this case, as the atmospheric effects are compensated from correctly calibrated imagery; however, this term has not yet been widely established.

In this section, some empirical normalization methods are summarized first, which allow for fast and efficient atmospheric correction. The basics of methods based on radiative transfer models are given in the subsequent subsections.

8.9.2.1 Empirical Reflectance Normalization

All empirical atmospheric correction methods have in common that a priori knowledge about the surface spectral albedo is put in relation to the imagery in order to find factors for a normalization of the atmospheric effect (Smith *et al*. 1987). Hereafter, a collection of methods that are suited for systems of unsecured calibration state and if fast results are required are compiled. These methods may be applied on uncalibrated image data, that is, directly on the digital number DN_s.

The flat-field approach (Dobbins and Boone, 1998) uses a spectrally flat spectrum from within the image for normalization to calculate a flat-field (quasi-) reflectance ρ_{ff} such that

$$\rho_{ff} = \frac{DN_s}{DN_{ff}} \tag{8.8}$$

where DN_s is the (uncalibrated) digital number signal at the sensor and DN_{ff} is the signal of a selected spectrum. This normalization may result in reflectance values above 100% as the selected flat-field reflectance is usually below 100 %.

The known/bright target approach uses the known (or assumed) reflectance ρ_b of one typically bright target in the image such that the whole (calibrated) image data may be normalized by the at-sensor measurement DN_b at the target by the transformation:

$$\rho = \frac{DN_s}{DN_b} \cdot \rho_b \tag{8.9}$$

A variation of the bright target approach is the ''quick atmospheric correction'' (QUAC) method (Bernstein *et al*. 2008). Instead of taking one pixel as a reference, the relation of a generic expected average reflectance to the average signal in the image is taken as reference for correction of the full image, also known as *IARR method* (Kruse, 1988).

The empirical line correction uses a combination between dark and bright targets in a scene. If two or more objects are known, a linear function is derived for each spectral band between measured signal and reflectance. The linear fit is performed between the known reflectances ρ_i and the respective measurements DN_i, such

that a slope $\Delta\rho/\Delta\mathrm{DN}$ of the function $\rho(\mathrm{DN})$ with a typical offset for dark objects $\mathrm{DN}_{\mathrm{dark}}$ can be found. This function is then used for normalization of all spectra of the image using the equation

$$\rho = (\mathrm{DN_s} - \mathrm{DN_{dark}}) \cdot \frac{\Delta\rho}{\Delta\mathrm{DN}} \tag{8.10}$$

The empirical line works satisfactorily well for flat terrain and small FOV imagery but is at its limit in mountainous areas and if repeatable corrections are required for an image series.

8.9.2.2 At-Sensor Radiance Description

Other than the empirical correction methods, the physical atmospheric correction of HRS data relies on an appropriate description of the at-sensor radiance from known parameters. In HRS, the at-sensor radiance is composed of three major components comprising the direct reflected and the backscattered radiance from the surface and the atmosphere. The thermal emission may be neglected for the wavelength range up to 2.50 µm as long as the temperature of the surface is below 350 K. Thus, the at-sensor radiance I_s may be in a good approximation described as a sum of the direct ground-reflected radiance $I_{g,dir}$, the so-called adjacency radiance $I_{g,adj}$, and the atmospheric radiance I_{atm}:

$$I_s = I_{g,dir} + I_{g,adj} + I_{atm} \tag{8.11}$$

We use ρ as the in-field hemispherical–directional reflectance factor (also denoted as $\mathrm{HDRF_{meas}}$), ρ_{adj} as the large-scale spectral albedo of the surface, and s as the spherical albedo of the atmosphere. The terms in Eq. (8.11) may then be written in a good approximation for the direct component

$$I_{g,dir} = \frac{1}{\pi} \cdot F_g \cdot \rho_g \cdot \tau_u \tag{8.12}$$

the adjacency radiance

$$I_{g,adj} = \frac{1}{\pi} \cdot F_g \cdot \rho_{adj} \cdot \tau_{u,adj} \tag{8.13}$$

and the atmospheric radiance

$$I_{atm} = \frac{1}{\pi} \cdot F_0 \cdot s \tag{8.14}$$

The term F_0 is the top-of-atmosphere irradiance and F_g is the total irradiance (solar flux) on a ground surface element, which may be written as

$$F_g = F_0 \cdot \tau_d \cdot \cos\varphi + F_{dif} \cdot V_{sky} + F_{ter} \tag{8.15}$$

The latter depends on the local solar incidence angle φ and includes the total diffuse irradiance F_{dif}, scaled by the fraction of the visible sky (skyview factor V_{sky}) and the terrain irradiance F_{ter}. The parameter τ_d is the downward atmospheric transmittance; τ_u and $\tau_{u,adj}$ are the upward transmittances of the atmosphere for the direct and the adjacency radiative paths, respectively.

A different formulation of the at-sensor radiance is derived, if the adjacency term is written using the back-reflected radiance from the ground coupled by the single scattering albedo s of the atmosphere, compare (Tanré *et al.* 1979). Here, all ground-reflected radiance is summarized in the term $I_{g,tot}$. This results in the following relation:

$$I_s = I_{g,tot} + I_{atm} = \tau_u \cdot F_g \cdot \rho_g \cdot \frac{1}{\pi \cdot (1 - \rho_{adj} \cdot s)} + I_{atm} \tag{8.16}$$

where the parameters are as described for Eq. (8.11). Such formulations of the at-sensor radiance are the basis for the atmospheric correction task.

8.9.2.3 Radiative-Transfer-Based Atmospheric Correction

Radiative transfer codes (RTCs) such as MODTRAN®-5 (Berk *et al.* 2005) or 6 S-V (Vermote *et al.* 2006) are well suited for forward simulation of the at-sensor signal from given boundary conditions. However, they are not built for the task of inversion for surface reflectance properties from radiometric images. For this purpose, atmospheric correction software is required. Examples of such software are TAFKAA (Gao *et al.* 2000), ACORN (Atmospheric Correction Now) (Green, 2001), HAATCH (High Accuracy Atmospheric Correction for HRS Data) (Qu, Goetz, and Heidbrecht, 2001), ATCOR (Atmospheric Topographic Correction) (Richter and Schläpfer, 2002), or FLAASH (Fast Line-of-Sight Atmospheric Analysis of Spectral Hypercubes) (Cooley *et al.* 2002). Such software allows an efficient inversion of the calibrated imagery on the basis of set of equations bellow. By inversion and reformulation of Eq. (8.11), the surface reflectance may be retrieved by the following equation:

$$\rho_g = \frac{\pi \cdot d^2 \cdot \left(I_s - I_{g,adj} - I_{atm}\right)}{\tau_u \cdot \left(\tau_d \cdot F_0 \cos\varphi + F_{dif} \cdot V_{sky} + F_{ter}\right)} \tag{8.17}$$

The components of this equation are to be derived from (i) physical model of a radiative transfer code: I_{atm}, F_{dif}, τ_d, and τ_u; (ii) boundary conditions of terrain: incidence angle φ and sky view factor V_{sky}; (iii) astronomical data: the average extraterrestrial solar constant F_0 and the dependency on the relative Earth–Sun distance described by parameter d; and (iv) iteration of atmospheric correction: $I_{g,adj}$ and terrain irradiance F_{ter}.

As all the parameters except F_0 and d vary per pixel, it is not feasible to calculate the radiative transfer directly for each pixel. Precalculated look-up tables (LUTs) are normally employed. These LUTs are interpolated with the pixel properties to find the applicable parameters for the correction.

A different approach is to perform the atmospheric compensation in the ''apparent reflectance'' domain ρ_s after dividing the at-sensor radiance by the ground

solar irradiance, propagated to the at-sensor level $F_{0,s}$:

$$\rho_{\mathrm{s}} = \frac{\pi \cdot d^2 \cdot I_{\mathrm{s}}}{F_{0,\mathrm{s}}} \tag{8.18}$$

$$\rho_{\mathrm{atm}} = \frac{\pi \cdot d^2 \cdot I_{\mathrm{atm}}}{F_{0,s}} \tag{8.19}$$

$$\rho_{\mathrm{adj}} = \frac{\pi \cdot d^2 \cdot I_{\mathrm{adj}}}{F_{0,s}} \tag{8.20}$$

These terms are typically used over flat ground, introducing a total transmittance term $\tau_{\mathrm{tot}} = \tau_{\mathrm{d}} \cdot \tau_{\mathrm{u}}$, which relates the at-sensor reflectance to the ground reflectance. The inversion of Eq. (8.16) for reflectance results in

$$\rho_{\mathrm{g}} = \frac{(\rho_{\mathrm{s}} - \rho_{\mathrm{atm}}) \cdot \left(1 - \rho_{\mathrm{adj}} \cdot s\right)}{\tau_{\mathrm{tot}}} \tag{8.21}$$

If the adjacency reflectance is further assumed to be the same as the pixel reflectance (i.e., $\rho_{\mathrm{adj}} = \rho_{\mathrm{g}}$), the equation is reduced to

$$\rho_{\mathrm{g}} = \frac{(\rho_{\mathrm{s}} - \rho_{\mathrm{atm}})}{\tau_{\mathrm{tot}} + (\rho_{\mathrm{s}} - \rho_{\mathrm{atm}}) \cdot s} \tag{8.22}$$

This is a basic atmospheric correction equation, which may be used in simple atmospheric correction programs or for fast inversion of a radiative transfer code. Note that working in the reflectance domain is critical for airborne instruments, as this approximation relies on accurate knowledge of the radiance at sensor level. An additional modeling step is required to infer the at-sensor radiance level $F_{0,s}$ as a reference value.

8.9.3 Process of Complete Atmospheric Correction

A complete atmospheric correction as implemented in atmospheric correction routines follows these steps: (i) create a LUT, containing the parameters of the above equations in relation to the parameters at a fixed number of data points (covering the expected range); (ii) calculate skyview factor, height, and incidence angle from DEM (digital elevation model), using the solar zenith and azimuth angles; (iii) derive atmospheric parameters from imagery (i.e., water vapor and aerosol load of the atmosphere); (iv) make fixed preselections (e.g., flight altitude and aerosol model); (v) invert the LUT, that is, derive the parameters by multilinear interpolation for each pixel; (vi) use Eq. (8.10) or (8.22) to perform the atmospheric correction; and (vii) perform the last two iteration of steps for adjacency correction and for the calculation of the terrain irradiance.

Some variations of this procedure exist, as the parameterization of the problem may differ and the LUT may be precalculated or calculated for each scene directly while correcting the data. An ideal high level standard procedure combines geometric and atmospheric processing (Schläpfer and Richter, 2002). Linked parameters are the viewing angle per pixel, the absolute distance from the aircraft to each

pixel location, or the relative air mass between sensor and pixel. Furthermore, other DEM related parameters, such as height, slope, or aspect, are required for radiometric correction algorithms and can only be used if the image is brought to the same geometry as the DEM. The dependencies within the atmospheric correction part lead to iterative reflectance retrieval steps, specifically for adjacency correction purposes. The final step of the processing should be a correction of the reflectance anisotropy (i.e., a BRDF correction). Some details regarding crucial correction steps are given hereafter.

8.9.3.1 Atmospheric Parameter Retrieval

Airborne HRS sensors offer the inherent capability for automatic retrieval of the radiometrically critical parameters atmospheric water vapor content and aerosol load (optical thickness). For the atmospheric water vapor, the 0.94/1.13 µm water vapor absorption bands are typically used for the retrieval of columnar water vapor over land on a per-pixel basis (Schläpfer *et al.* 1998). The aerosol optical thickness is normally calculated using the dark dense vegetation (DDV) approach (Kaufman and Tanré, 1996) interpolating the aerosol load to areas not covered by vegetation. These two methods allow for a mostly autonomous atmospheric correction of HRS data.

8.9.3.2 Adjacency Correction

The correction of the atmospheric adjacency effect is of high relevance, especially for limnological applications (Tanré *et al.* 1987). The effect is significant in a horizontal range from 100 m up to 1.5 km starting at flight altitudes of 1000 m above ground and higher. Thus, each pixel has to be corrected with respect to the average reflectance of the adjacent areas. This can be carried out in an efficient way by the definition of a spatial convolution function, which takes a distance-weighted average of the adjacent area in the image to calculate an adjacency weighting factor. The corresponding radiance has to be simulated in the radiative transfer code as indirect ground-reflected radiance according to the aforementioned parameterization.

8.9.3.3 Shadow Correction

Cast shadows, cloud shadows, and shadows from building are often present in HRS data. They receive mostly diffuse irradiance that is sufficient to provide enough signal for data analysis with state of the art sensor systems. Correction approaches try to classify the shadowed areas first and then apply a separate correction model to these parts of the image such that shadows are removed in optimal situations (Adler-Golden *et al.* 2002; Richter and Muller, 2005). The correction model takes into account the diffuse nature of the irradiance in the cast shadow areas and needs to consider the skyview factors correctly for an accurate correction.

8.9.3.4 BRDF Correction

The derivation of spectral albedo (i.e., the bihemispherical reflectance, BHR) from directional reflectance values is the task of BRDF correction. The operational correction of BRDF effects in images is not yet solved satisfactorily, but progress

has been made on this issue (Feingersh, Ben-Dor, and Filin, 2010). The correction of the BRDF effects may be performed if the BRDF properties of the observed target(s) and the (diffuse) irradiance distribution is known. For operational use, an anisotropy factor needs to be calculated and applied for each pixel. This factor accounts for the relation between measured hemispherical–directional reflectance ($HDRF_{meas}$) and the spectral albedo (BHR; also known as *white sky albedo*). The anisotropy factor has to be inferred from an appropriate BRDF model or from measurements. The finally calculated spectral albedo product is a quantity that may be easily compared in multitemporal analysis and may be used for unbiased object classification.

8.9.4 Retrieval of Atmospheric Parameters

On the basis of the relatively high spectral resolution obtain by the HRS sensors, one can use the specific absorption features of atmospheric gases (natural or contaminated) and evaluate their column content on a pixel-by-pixel basis. This may provide an innovative way of mapping the gases' spatial distribution and of spotting new quantitative information on the atmospheric conditions at very high spatial resolution. The gases that are active across the UV-VIS-NIR-SWIR-TIR spectra are divided into two sectors: (i) a major sector in which the spectral response of the gases is well detected (high fraction and strong absorption) and (ii) a minor sector in which the spectral response is low and difficult to assess because of the low fraction of the gases and relatively weak absorption features. The major gas group is composed of O_2, H_2O, and CO_2, whereas the minor gas group consists of O_3, N_2O, CO, and CH_3 in the UV-VIS-NIR-SWIR and SO_2 and NO_2 in the TIR. Figure 8.7 provides the absorptance features of the above gas components across the UV-VIS-NIR-SWIR-TIR spectral region along with the atmospheric windows. The advantage of assessing the above gases on a pixel-by-pixel basis is significant. It can help accurately extract surface reflectance by estimating the gases' absorption (and hence their atmospheric transmission) on a pixel-by-pixel column basis. Consequently, calculating water vapor directly from the image, first demonstrated by Gao and Goetz (1995), is now a very common way of achieving high performance of atmospheric correction methods (Section 8.8). While H_2O is considered to be a nonuniformly spatially distributed gas, other major gases, that is, CO_2 and O_2, are known to be well mixed – hence, their use as indicators to assess atmospheric phenomena that might affect the spatial distribution of the gas in question. For example, over rough terrain, if spatial changes are encountered using a well-mixed gas, this might indicate different elevations, as the column pixel volume over high terrain consists of less molecules than that over low terrains for a particular gas. On the basis of this, Ben-Dor and Kruse (1996) and Green (2001) showed that it is possible to construct a DEM structure of the studied area solely from the HRS radiance information and the CO_2 peak. Furthermore, as O_2 is also a well-mixed gas, it can be used to estimate, on a pixel-by-pixel basis, the Mie scattering effect across the VIS–NIR region and hence can be used to better extract

the surface reflectance, assuming that the scattering is not a spatially homogeneous phenomenon. Using one absorption peak of the H_2O at 1.38 μm, Gao, Goetz, and Wiscombe (1993) showed that a nonvisible cirrus cloud can be detected and mapped based on the high scattering properties of the ice particles within the cloud volume. Ben-Dor (1994) suggested taking precautions in using these absorption peaks over high terrain and bright targets, and in another paper, (Ben-Dor, Goetz, and Shapiro, 1994) suggested that the O_2 peak be used to map the cirrus cloud distribution in the VIS–NIR region (0.760 μm). On the basis of this idea, Schläpfer *et al.* (2006) was able to quantitatively assess a smoke plume over a fire area using the scattering effect on the O_2 absorption peak. Alakian, Marion, and Briottet (2008) developed a method to retrieve the microphysical and optical properties in aerosol plumes (L-APOM) in the VIS region as well. Recently, Chudnovsky *et al.* (2009) mapped a dust plume over the Bodele depression in northern Chad using Hyperion data and the SWIR region. Another innovative study that shows the applicability of HRS in the atmosphere was performed by Roberts *et al.* (2010). They showed that if high SNR data are available, it is also possible to detect the distribution of minor gases. Using AVIRIS 2006 data over a marine (dark) environment, they were able to detect, on a pixel-by-pixel basis, the emission of methane over the Coal Oil Point (COP) marine seep fields, offshore of Santa Barbara, California, and the La Brea Tar Pits in Los Angeles, California. In the TIR region, there are several examples of the detection of plumes of toxic gases based on the fundamental vibration peak across the atmospheric windows between 2.5 and 16 μm. Using SO_2 emission in the LWIR region at 8.58 and 8.82 μm, Shimoni *et al.* (2007) were able to spot shade on a plume emitted over an industry refinery zone with additional information extracted from the VIS region. Figure 8.7 provides a summary for the absorption positions of some of the above mentioned gases across the VIS-NIR-SWIR-TIR spectral region. In summary, it can be concluded that HRS technology is not only capable of deriving surface information but also has the proven capability to extract quantitative information on atmosphere constituents in an innovative way that none of the current remote sensing means can provide.

8.9.5
Mapping Methods and Approaches

Over the past few years, many techniques for mapping and processing of HRS data have been developed (Schaepman *et al.* 2009). The special characteristics of hyperspectral data sets pose different processing problems, which must be tackled under specific mathematical formulations, such as classification (Landgrebe, 2003; Richards and Jia, 2006) or spectral unmixing (Adams, Smith, and Johnson, 1986). These problems also require specific dedicated processing software and hardware platforms (Plaza and Chang, 2007).

In previous studies (Plaza *et al.* 2009), available techniques were divided into full-pixel and mixed-pixel techniques, where each pixel vector defines a spectral signature or fingerprint that uniquely characterizes the underlying materials at each site in a scene. Mostly based on previous efforts in multispectral imaging,

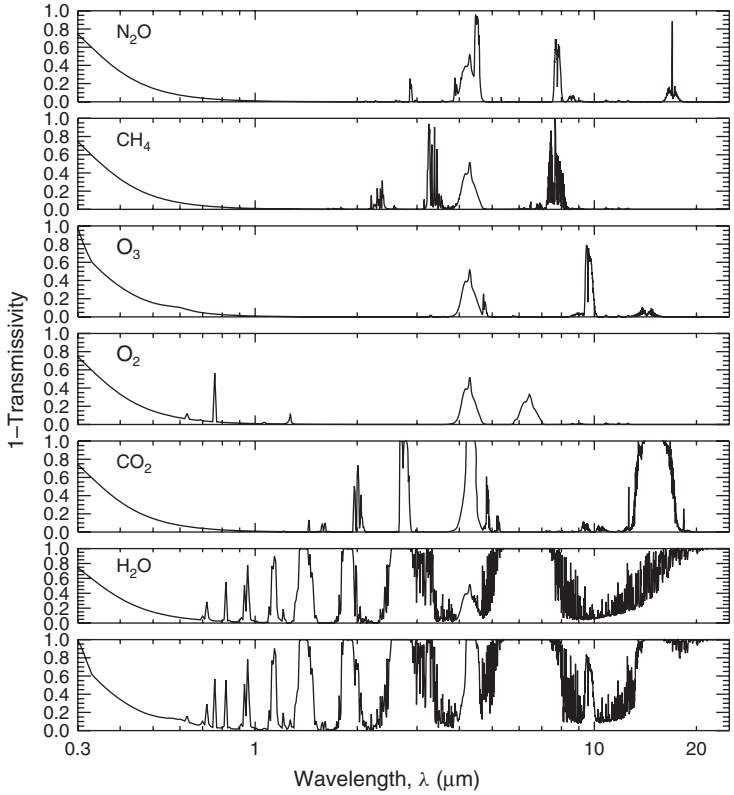

Figure 8.7 Extinction spectra of atmospheric gases across the VIS-NIR-SWIR-TIR region. The simulations were performed with MODTRAN4 (version 3 Revision 1, MOD4v3r1), with the Sun in the zenith; the spectral results were averaged over a FWHM of 10 nm. (Source: Adapted from Wendisch and Yang (2012).)

full-pixel techniques assume that each pixel vector measures the response of one single underlying material (Schaepman *et al.* 2009). Often, however, this is not a realistic assumption. If the spatial resolution of the sensor is not good enough to separate different pure signature classes at the macroscopic level, these can jointly occupy a single pixel, and the resulting spectral signature will be a composite of the individual pure spectra, often called *endmembers* in hyperspectral terminology (Boardman, Kruse, and Green, 1995). Mixed pixels can also result when distinct materials are combined into a homogeneous or intimate mixture, which occurs independently of the spatial resolution of the sensor. To address these issues, many spectral unmixing approaches have been developed under the assumption that each pixel vector measures the response of multiple underlying materials (Kruse, 1988; Keshava and Mustard, 2002).

Spectral unmixing has been an alluring goal for exploitation, from the earliest days of hyperspectral imaging (Goetz *et al.* 1985) until today. Regardless of the spatial resolution, the spectral signatures collected in natural environments are

invariably a mixture of the signatures of the various materials found within the spatial extent of the ground instantaneous field view of the imaging instrument (Adams, Smith, and Johnson, 1986). In this case, the measured spectrum may be decomposed into a combination of pure spectral signatures of soil and vegetation, weighted by areal coefficients that indicate the proportion of each macroscopically pure signature in the mixed pixel (Keshava and Mustard, 2002). The availability of hyperspectral imagers with a number of spectral bands exceeding the number of spectral mixture components (Green *et al.* 1998) has allowed casting the unmixing problem in terms of an over determined system of equations in which, given a set of pure spectral signatures (called endmembers), the actual unmixing to determine apparent pixel abundance fractions can be defined in terms of a numerical inversion process (Harsanyi and Chang, 1994; Bateson and Curtiss, 1996; Plaza *et al.* 2004; Berman *et al.* 2004; Chang *et al.* 2006; Rogge *et al.* 2006; Wang and Chang, 2006; Zaer and Gader, 2008).

A standard technique for spectral mixture analysis is linear spectral unmixing (Heinz and Chang, 2001; Plaza *et al.* 2004), which assumes that the spectra collected by the spectrometer can be expressed in the form of a linear combination of endmembers weighted by their corresponding abundances. It should be noted that the linear mixture model assumes minimal secondary reflections and multiple scattering effects in the data-collection procedure, and hence, the measured spectra can be expressed as a linear combination of the spectral signatures of materials present in the mixed pixel (Figure 8.8a). Although the linear model has practical advantages, such as ease of implementation and flexibility in different applications (Chang, 2003), nonlinear spectral unmixing may best characterize the resultant mixed spectra for certain endmember distributions, such as those in which the endmember components are randomly distributed throughout the instrument's FOV (Guilfoyle, Althouse, and Chang, 2001). In those cases, the mixed spectra collected by the imaging instrument are better described by assuming that part of the source radiation is multiply scattered before being collected at the sensor (Figure 8.8b). In addition, several machine-learning techniques have been applied to extract relevant information from hyperspectral data during the past decade. Taxonomies of remote sensing data-processing algorithms (including hyperspectral analysis methods) have been developed in the literature (Richards and Jia, 2006 Schowengerdt, 1997). It should be noted, however, that most available hyperspectral data-processing techniques focus on analyzing the data without incorporating information on the spatially adjacent data, that is, hyperspectral data are usually not treated as images but as unordered listings of spectral measurements with no particular spatial arrangement (Rogge *et al.* 2006). The importance of analyzing spatial and spectral patterns simultaneously has been identified as a desired goal by many scientists devoted to multidimensional data analysis.

In certain applications, however, the integration of high spatial and spectral resolution is mandatory to achieve sufficiently accurate mapping and detection results. For instance, urban area mapping requires sufficient spatial resolution to distinguish small spectral classes, such as trees in a park or cars on a street (Bruzzone and Marconcini, 2006). Owing to the small number of training samples

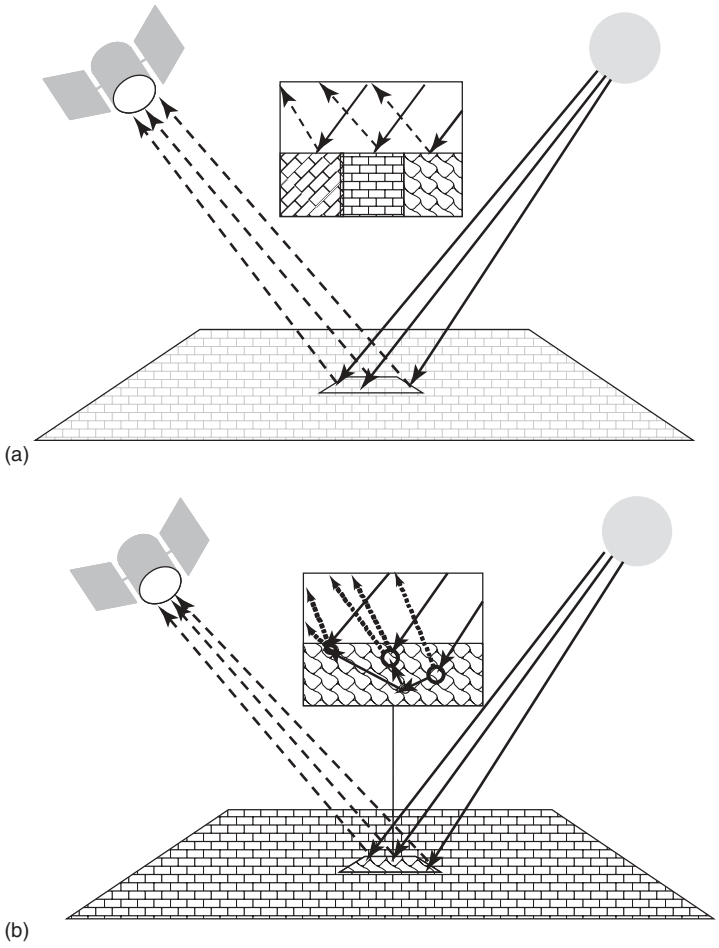

Figure 8.8 Linear (a) versus nonlinear (b) mixture models: single versus multiple scattering.

and the high number of features available in remote sensing applications, reliable estimation of statistical class parameters is another challenging goal (Foody, 1999). As a result, with a limited training set, classification accuracy tends to decrease as the number of features increases. This is known as the *Hughes effect* (Landgrebe, 2003). High-dimensional spaces have been demonstrated to be mostly empty, thus making density estimation even more difficult. One possible approach to handling the high-dimensional nature of hyperspectral data sets is to consider the geometrical properties rather than the statistical properties of the classes. The good classification performance demonstrated by support vector machines (SVMs) using spectral signatures as input features (Prasad, 2008) can be further increased by taking advantage of semisupervised learning and contextual information. The latter is performed through a combination of kernels dedicated to spectral and

contextual information, while in the former, the learning is provided with some supervised information in addition to the wealth of unlabeled data. Among the great many methods proposed in the literature for such approaches, we focus on the transductive SVM for semisupervised learning (Bruzzone and Marconcini, 2006) or a composite kernel-based methodology for contextual information integration at the kernel level (Camps-Valls *et al.* 2006) have shown great success in practice.

As most of the methods reviewed here deal with endmember extraction and data mining from the reflectance or emittance cubes (an unsupervised approach), there are methods in which the endmembers are known in advance or the spectral model to map the pixels has already been developed (supervised approach). One of the first and most usable endmember-based approaches in HRS is the Spectral Angle Mapper (SAM), developed by Kruse *et al.* (1993), which is based on the angle calculated between two spectral vectors: the pixel and the selected endmember. Since then, many other spectral-based techniques have been developed, where most recently, spectral-based models that are generated in a spectral domain (e.g., PLS or neural network) are implemented on a pixel-by-pixel basis to the image cube in question. This method enables quantitative mapping of selected properties on the Earth's surface such as infiltration rate (Ben-Dor *et al.* 2004) organic matter content (Stevens *et al.* 2008), salinity (Ben-Dor *et al.* 2002), and more.

Finally, although the mapping and classification techniques described above hold great promise for hyperspectral data processing, they also introduce new computational challenges. With the recent explosion in the amount and complexity of hyperspectral data, parallel processing and high-performance computing (HPC) practices have necessarily become requirements in many remote sensing missions, especially with the advent of low-cost systems such as commodity clusters (Plaza and Chang, 2007). On the other hand, although hyperspectral analysis algorithms map nicely to clusters and networks of workstations, these systems are generally expensive and difficult to adapt to on-board data-processing requirements introduced by several applications, such as wildland fire tracking, biological threat detection, monitoring of oil spills, and other types of chemical contamination. In those cases, low-weight and low-power integrated components are essential to reducing the mission's payload and obtaining analyzed results quickly enough for practical use. In this regard, the emergence of specialized hardware devices such as field-programmable gate arrays (FPGAs) has helped in bridging the gap toward real-time analysis of remotely sensed hyperspectral data.

8.10 Sensor Calibration

8.10.1 General

In combination, calibration and validation (cal/val) can be regarded as a single process that encompasses the entire remote sensing system, from sensor to data

product. The objective of both is to develop a quantitative understanding and characterization of the measurement system and its biases in both space and time (National Research Council, 2007). Calibration of hyperspectral sensor data is a critical activity for a number of reasons. First, we need to have confidence in the reliability of data delivered by such sensors. Second, as many of the products that we are deriving from hyperspectral data are quantitative, we need to know that the data from which they are derived are accurate (this holds for qualitative data as well). We often test the accuracy of remote sensing data products by performing validation of the subsequent data sets; thus, the raw data delivered by sensors must be well calibrated and the products derived from them are also well validated. cal/val are, therefore, activities that form an integral component of the efficient use of any form of EO data and in the maintenance of the scientific value of EO data archives. As HRS data are acquired in DN values, but for most applications, we need radiometric information as an input to extract reflectance or emissivity values, accurate transfer from one stage to another is crucial. In this respect, radiometric and spectroscopic assurance is required. Radiometric calibration refers to the process of extracting physical units from the original raw spectroscopic data and assigning the channels in the sensors to a meaningful wavelength.

Cal/val is, therefore, a fundamentally important scientific activity and should be a continuous component in any remote sensing program, providing an independent check on the performance of both space-based airborne and ground-based hyperspectral sensors and processing algorithms.

In general, one can say that the calibration of EO data is critical if we are to reliably attribute detected changes observed in data to real environmental changes occurring at ground level. Without calibration, we are unable to rule out the influence of other factors, such as instrument error or influences of the atmosphere. This problem is exacerbated by the myriad of sensors operated by multiple countries and organizations. Calibration allows the traceability of sensor data to the same physical standards and is routinely required as sensors decay throughout their lifetime. Calibration is thus critical if we want to reliably extract information from measured radiance, compare information acquired from different regions and different times, compare and analyze HRS observations with measurements provided by other instruments, and extract information from spectral image measurements using physically based computer models.

Validation refers to the independent verification of the physical measurements made by a sensor as well as the derived geophysical variables. Validation allows for the verification and improvement of the algorithms used (e.g., for atmospheric correction and vegetation state). To achieve this, conventional, ground-based observations are required using calibrated and traceable field instrumentation and associated methods. To this end, several indicators are valid and developed to check the accuracy of the calibration stage and provide the user with a reliable feeling about his data set.

The definition of all the common terms used here for cal/val are taken from the Committee of Earth Observation Satellites (CEOS) as follows:

(i) *Calibration*. The process of quantitatively defining the responses of a system to known, controlled signal inputs;
(ii) *Validation*. The process of assessing, by independent means, the quality of the data products derived from the system outputs;
(iii) *Traceability*. Property of a measurement result relating the result to a stated metrological reference (free definition and not necessarily SI) through an unbroken chain of calibrations of a measuring system or comparisons, each contributing to the stated measurement uncertainty;
(iv) *Uncertainty*. Parameter that characterizes the dispersion of the quantity values that are being attributed to a measured mean, based on the information used;
(v) *Vicarious Calibration*. Vicarious calibration refers to techniques that make use of natural or artificial sites on the surface of the Earth for post calibration of airborne or spaceborne sensors.

8.10.2 Calibration for HSR Sensor

Calibration translates electrical output DN values (voltages or counts) to reliable physical-based units (radiometric information) by determining the transfer functions and coefficients necessary to convert a sensor reading. The coefficients are extracted throughout a careful measurement stage in the laboratory using well-calibrated facilities and traceable standards. There are a number of components ensuring a thorough calibration approach. Radiometric and spectral responses need to be accurately monitored through the lifetime of a sensor to monitor changes in response, as it ages over time. In the case of spaceborne hyperspectral sensors, both prelaunch and post (on-orbit) launch calibrations are undertaken, either directly or using vicarious targets-on-orbit and vicarious calibration enable taking into account changes in calibration over time using the moon's surface (Kieffera *et al.* 2003). Airborne hyperspectral sensors have the advantage over spaceborne sensors that they can be removed from the aircraft and resubjected to rigorous laboratory calibration tests similar to those performed for prelaunch calibration of spaceborne sensors. This is often performed before and after a flying ''season.'' The calibration coefficients from each season can also be used to track the sensor's deterioration over its years of operation.

8.10.2.1 Preflight Calibration

The three key components to prelaunch calibration are radiometric, spectral, and spatial. Achieving radiometric calibration involves the use of a calibrated integrating sphere whose ideal output is homogeneous and large enough to illuminate all elements in a sensor array with the same radiance. An absolute radiometric calibration determines the relationship between sensor signals and radiance for all spectral channels. Varying the output of the integrating sphere also allows for the study of the linearity between sensor response and radiance and the assessment of the SNR at radiance levels similar to those encountered when sensing the Earth's surface (Gege *et al.* 2009).

Spectral calibration typically uses a monochromator to produce a collimated narrow beam of light that is blocked by transmission filters and is thus tunable to different wavelengths. Measurements performed here allow for determination of spectral response function, center wavelength, spectral smile, spectral sampling distance, the spectral range of pixels, and spectral resolution and to perform a wavelength calibration (Oppelt and Mauser, 2007).

Spatial calibration (geometric) can most accurately be achieved with the movement of a point light source across the sensor array whose beam is controlled by a slit (Gege *et al*. 2009). This allows for along-track and across-track calibration of the sensor array. Measurements performed here allow for the derivation of line spread function across track; center coordinates for each CCD in the array; across-track sampling distance; pixel instantaneous FOV; total sensor FOV; and the modulation transfer function (the reparability of adjacent targets as a function of distance and contrast (Oppelt and Mauser, 2007).

8.10.2.2 **In-Flight/In-Orbit Calibration**

This involves the use of in-built calibration sources and vicarious calibration or cross-calibration to other satellite sensors. The critical issue at this stage is to be able to monitor changes in sensor performance over time (Pearlman *et al*. 2003). For example, Hyperion, the first fully spaceborne hyperspectral sensor, relied on the diffuse reflectance of an in-built Spectralon ™reflectance surface illuminated by the Sun or a lamp, in calibrations performed once every two weeks. The moon and other opportunistic Earth surface targets were also used to monitor sensor performance over time (Jarecke and Yokoyama, 2000; Pearlman *et al*. 2003; Ungar *et al*. 2009). Cross-calibration to data from the LANDSAT 7 ETM+ sensor was also frequently performed.

EnMAP, the new German-built hyperspectral sensor scheduled for launch in 2015, will carry for calibration a full aperture diffuser, coupled with an integrating sphere with various calibration lamps. A shutter mechanism also allows for dark measurements to be performed. APEX, a joint Belgian–Swiss airborne sensor development, carries an in-flight characterization facility using a stabilized lamp coupled with vicarious and cross-calibration (Nieke *et al*. 2008), (Itten *et al*. 2008).

8.10.2.3 **Vicarious Calibration**

Vicarious calibration is also used as an in-flight check on sensor performance (Green and Shimada, 1997; Green and Pavri, 2000; Secker *et al*. 2001). The approach can use homogeneous targets on the land surface (e.g., dry lake beds, desert sands, ice sheets, water bodies, and so on) or artificial targets of varying brightness if the sensor has sufficient spatial resolution (Brook and Ben-Dor, 2011). The sites or targets must be well characterized, and ideally, reflectance and, if possible, radiance should be measured at the ground surface using calibrated spectroradiometers simultaneously with sensor overflight. Increasingly sophisticated ground-based instrumentation is being used to provide autonomous and near-continuous measurement of the characteristics at many of these sites (Brando *et al*. 2010). Correction involves either top-down (correction of ''top-of-atmosphere''

sensor data to ground-leaving reflectance using an atmospheric correction model) or bottom-up (correction of ground target reflectance to top-of-atmosphere radiance using a radiative transfer model taking into account atmospheric transmission and absorption, e.g., MODTRAN). Increasingly, a combination of measurements obtained at varying scales and resolutions (e.g., *in situ*, airborne, and satellite) are being used to provide the basis for assessment of the on-orbit radiometric and spectral calibration characteristics of spaceborne optical sensors (Green, Pavri, and Chrien, 2003a).

The smaller pixel sizes of airborne imagery compared to typical image satellite resolutions, along with targeted deployment, means that artificial vicarious calibration targets can be rapidly deployed in advance of specific airborne campaigns. Such targets can also help overcome the difficulties of finding sufficient natural homogeneous targets of varying brightness. Supervised vicarious calibration (SVC) (Brook and Ben-Dor, 2011) uses artificial agricultural black polyethylene nets of various densities as calibration targets, set up along the aircraft's trajectory. The different density nets, when combined with other natural bright targets, can provide full coverage of a sensor's dynamic range. The key to the use of any form of vicarious calibration target is the use of simultaneous field-based measurement of their reflectance properties and positions; uncertainties are reduced if a number of calibration targets are used, a large number of reflectance measurements are made of each target, and their positions are accurately located (Secker *et al*. 2001).

Vicarious calibration, therefore, provides an indirect means of QA of remotely sensed data and sensor performance that is independent of direct calibration methods (use of on-board radiance sources or panels). This is important as on-board illumination sources may themselves degrade over time.

In all calibration efforts, traceability, the process of ensuring measurements, is related through an unbroken chain of comparisons to standards held by National Metrology Institutes (e.g., National Institute of Standard and Technology (NIST), USA; PTB, National Standards Laboratory, Germany; and National Physics Laboratory (NPL), UK), is the key to allowing true intercomparability between different sensors' raw and product data sets (Fox, 2004). The chain is implemented via the use of ''transfer standards'' that allow traceability back to official ''primary'' radiometric standards using internationally agreed-upon systems of units (SI) and rigorous measurement and test protocols. Integral to the establishment of traceability is the quantification and documentation of associated uncertainties throughout the measurement chain; the fewer the number of steps in the chain, the lower the uncertainty. The advantages of maintaining traceability include a common reference base and quantitative measures of assessing the agreement of results for different sensors or measurements at different times. However, current traceability guidelines lack guidance on temporal overlap or interval length for the measurements in the unbroken chain of comparisons (Johnson, Rice, and Brown, 2004).

The successful implementation of cal/val activity needs careful planning of issues such as coordination of activities, selection and establishment of networks of sites, the development and deployment of instrumentation to support

measurement campaigns, the adoption of common measurement, and data distribution/availability protocols.

8.11 Summary and Conclusion

This chapter provides a snapshot of the emerging HRS technology. Although many aspects of this promising technique are not covered herein, we hope to have provided the reader with a sense of its potential for the future, as evidenced by past accomplishments. Besides being a technology that can provide added value to the remote sensing arena, it is an expansion of the spectroscopy discipline that has been significantly developing worldwide for many years. Very soon, when sensors in air and orbit domains begin to provide SNR values that are similar to those acquired in the laboratory, all spectral techniques available today will be able to implement the HRS data and forward the applications in a generation or two. HRS technology is emerging and the general scientific community use is growing. The number of sensors is also on the rise and new companies are entering into commercial activities. The most important step in the processing of HRS data is to obtain accurate reflectance or emissivity information on every pixel in the image; at that point, a sophisticated analytical approach can be used. This means that besides the atmospheric correction method, the data has to be physically reliable and stable at the sensor level. Mixed-pixel analysis and spectral models to account for specific questions are only a few examples of what this technology can achieve. The forthcoming HRS sensors in orbit are expected to drive this technology forward by providing temporal coverage of the globe at low cost and showing decision makers that the technology can add much to other space missions. The growing sensor-development activity in the market will also permit a ''sensor for all,'' which will also push the technology forward. As many limitations still exist, such as the TIR region not being fully covered, the information only being obtainable from a very thin layer, the time investment, high cost of data processing, and great effort needed to obtain a final product, investment in this technology is worthwhile. If the above limitations can be overcome, and other sensors' capabilities merged with it, then HRS technology can be the vehicle to real success, moving from a scientific demonstration technology to a practical commercial tool for remote sensing of the Earth.